CRITICAL SPEEDS OF A ROTATING SYSTEM WITH FLEXIBLE, DAMPED SUPPORTS

RAY F. CRATER

CRITICAL SPEEDS OF A ROTATING SYSTEM WITH FLEXIBLE, DAMPED SUPPORTS

*****

Ray F. Crater

CRITICAL SPEEDS OF A ROTATING SYSTEM WITH FLEXIBLE, DAMPED SUPPORTS

by

Ray F. Crater
Lieutenant, United States Navy

Submitted in partial fulfillment of
the requirements for the degree of

MASTER OF SCIENCE
IN
AERONAUTICAL ENGINEERING

United States Naval Postgraduate School
Monterey, California

1962

CRITICAL SPEEDS OF A ROTATING SYSTEM WITH FLEXIBLE, DAMPED SUPPORTS

by

Ray F. Crater

This work is accepted as fulfilling
the thesis requirements for the degree of

MASTER OF SCIENCE
IN
AERONAUTICAL ENGINEERING

from the

United States Naval Postgraduate School

ABSTRACT

An experimental and theoretical analysis of a rotating system with flexibly supported, viscously damped bearings is described. The theoretical development is based on the differential equations of motion of the mass of the rotor and the two shaft bearings. Tests were conducted and compared with calculated response of the system. Results indicate fair agreement The discrepancies are attributed to limited accuracy of test measurements and/or erratic operation of the viscous damping dashpots.

This work was conducted at the U. S. Naval Postgraduate School, Monterey, California.

TABLE OF CONTENTS

Table of Contents

LIST OF FIGURES

List of Figures

1 INTRODUCTION

The problem of vibration in rotating systems has commanded the attention of theoreticians and practical investigators for many years. With the advent of high speed marine turbines and turbo-jet aircraft engines renewed interest has been shown in this field.

It is well known that at certain speeds of rotation small imbalances tend to set up vibrations of large amplitudes in a rotating system. Prohl, who has made several contributions in this area, [1,2], wrote,

> The existing methods for determining critical speeds are subject to the following limitations. On one hand the methods that are general, i.e., that permit the calculations of higher speeds as well as the fundamental, involve calculations so complicated as to be impractical for any but the simplest of rotors. On the other hand, the methods for which the calculations are comparatively simple, such as the more familiar methods of Rayleigh and Stodola, lack generality in that critical speeds other than the fundamental cannot be definitely determined.

This criticism may have been well taken at the time. The large number of prime variables in any but the simplest system tend to confine most investigations to a very narrow scope; for example, "On Critical Speeds of a Shaft Supported by a Ball Bearing", by T. Yamamoto, which appeared in the Journal of Applied Mechanics of June, 1959. Doctor Yamamoto investigated two kinds of critical speeds induced by a slight difference in the diameter of the balls in their races.

A growing appreciation of modern computer capabilities has led to the development of increasingly general treatments such as, "Natural Frequencies of Nonuniform Beams on Multiple Elastic Supports", by R. A. DiTaranto of the Defense Electronics Products Division of Radio Corporation of America, [3]. An especially general and pertinent method was described recently by Messrs. Koenig, Guenther and Lovejoy of the Engineering Analysis Section, Allis-Chalmers Manufacturing Company, [4]. A concluding, third part of this method, as yet unpublished, is to include experimental results and correlation with the analytical method described

The study presented here investigates the transverse motion of a rotor on a flexible shaft. The motion of the two flexibly supported end bearings, which are subject to damping, is also studied.

The study includes both a practical investigation conducted with a machine designed specifically for this purpose and a theoretical analysis developed along parallel lines.

The theoretical analysis begins with the basic equations of motion. This approach was considered preferable to a mechanical application of one of the existing schemes of analysis.

The analytical model was constructed with the assumption that the rotor was the only rotating member. The shaft was considered to be massless and torsionally rigid. The speed of rotation was taken to be constant. Damping was assumed to be a linear function of the velocity.

This work was conducted at the U. S. Naval Postgraduate School, Monterey, California during the 1961-1962 academic year.

The author wishes to express his appreciation to Professors T. H. Gawain and M. H. Vavra and to the supervisory and laboratory personnel of the Department of Aeronautics of the U. S. Naval Postgraduate School.

2 TABLE OF SYMBOLS

A	general constant Fortran array
a	rotor position measured from left-hand support, in.
C	(1, 2, etc.) Fortran physical constant (A, E) Fortran damping constant
c	symmetrical damping constant, lbs./(in./sec.)
D	displacement, in. mean spring diameter, in.
d	wire diameter, in.
F	force, lbs.
G	shear modulus, lbs./sq. in.
g	gravitational constant, 386 in./sec.^{2}
I	diametral moment of inertia, in.^{4}
i	imaginary, $(-1)^{\frac{1}{2}}$
K,k	spring constant, lbs./in.
ℓ	shaft length, in.
m	mass, lbs.-sec.^{2}/in.
N	number of working coils of spring
N_1	first critical speed, RPM
P	load, lbs.
Q	general constant
R	general constant
t	time, sec.
W	weight, lbs.
w	rim weight, lbs.
$\bar{x}$	displacement of rotor c.g. from polar axis, in.
x	displacement, in.
$\dot{x}$	velocity, in./sec
$\ddot{x}$	acceleration, in./sec.^{2}
Z	general constant

Table of Symbols

δ	complex root
ϵ	rotor eccentricity, in.
λ	damping factor, $sec.^{-1}$
μ	mass ratio
μ_T	$\mu_1 + \mu_3$
ξ	$\mu_1 \mu_3$
π	3.1416
ϕ	phase angle, degrees
ω	angular frequency, radians/sec.

Subscripts:

1	left-hand bearing complex
2,R	rotor
3	right-hand bearing complex
d	damping
I	inertia
T	total

Abbreviations:

c.g	center of gravity
cps	cycles per second
in.	inches
lbs.	pounds
m.u.	mass units
RPM	revolutions per minute
sec.	seconds
sq.in.	square inches

3. THE PHYSICAL SYSTEM

A schematic drawing of the physical system is shown in Fig. 1. Detailed drawings from which the critical speed test rig was constructed are included in Appendix A.

3.1 Critical Speed Rig Design Concept

Bearings and restraints of high-speed rotating systems should be designed with great care. Bearings are normally confined as rigidly as possible in order to reduce the degrees of freedom of the system and to eliminate critical speeds below the operating speed range. However, shaft and bearing flexibility are inevitable due to the elastic nature of materials, oil film "stiffnesses", necessary clearances and machining tolerances. Similarly, imbalances due to imperfections and lack of homogeneity of shaft and rotor materials are always present to some degree. Even after exhaustive balancing procedures have been carried out some imbalances remain and contribute harmonic excitations in rotating systems.

The term impedance is sometimes used in describing the characteristics of spring and damping device combinations which act at the supports of a system. As noted by Guenther and Lovejoy, [4], support mechanical impedance can be, and is often, expressed as a function of not only the static properties of a system but of the operating speed as well.

In the case where support is provided by a simple spring, support stiffness is merely the familiar spring constant (force per unit deflection). The ideal mechanical spring acts as a conservative member in the system; energy stored in compression or tension is returned to the system when the spring returns to its unstrained state. Hysteresis losses present in actual springs are generally small and can be disregarded.

For the simple, damped, spring-mass system as discussed in most basic vibration texts, e.g., [5], a dashpot is shown as a device which develops forces opposing motion, the force so developed being proportional to the velocity. A dashpot acts as a non-conservative member dissipating energy from the system.

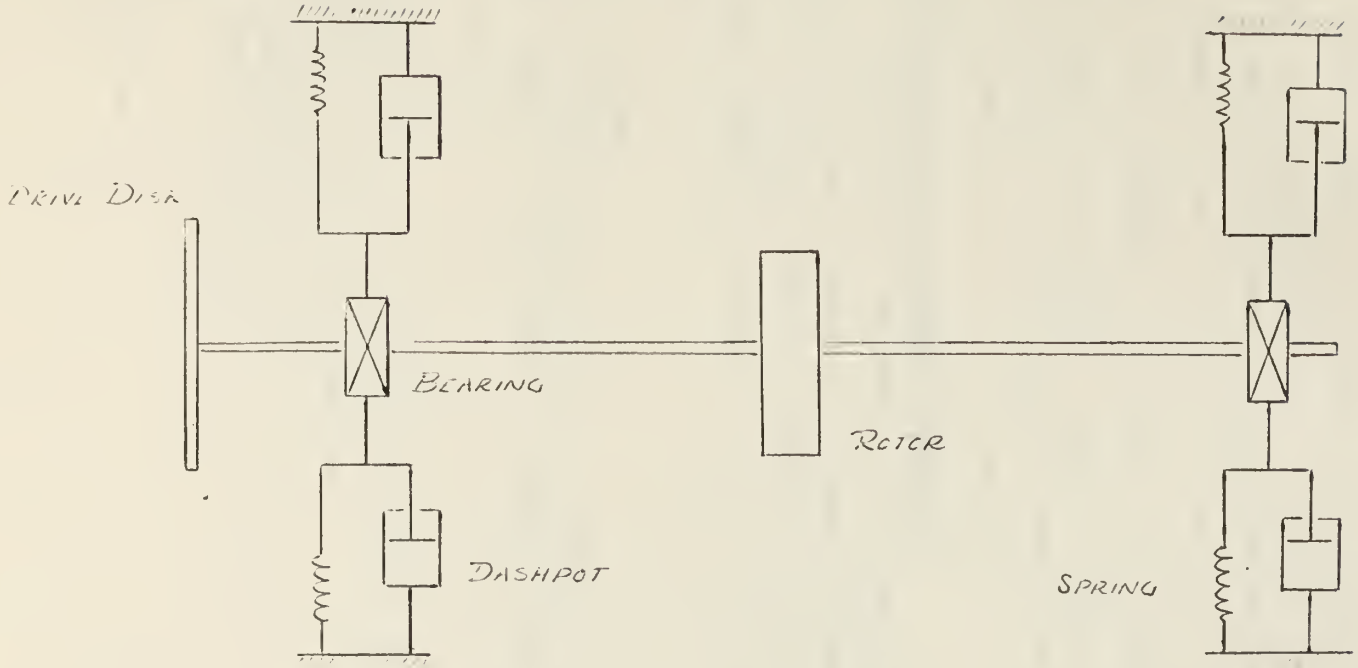

FIGURE 1

SCHEMATIC DRAWING OF PHYSICAL SYSTEM

Both the spring and the dashpot influence the critical speed(s). The dashpot governs the amplitudes associated with critical speed vibrations

The critical speed test rig was designed to provide a vehicle for practical investigation of the effects of support flexibility and viscous damping on the critical speeds and mass vibration amplitudes of a rotating system.

The salient points of the design with respect to its particular service are: (a) compressed air drive as opposed to mechanical drive which would constrain the shaft during vibration, and, (b) ability to control dashpot stiffness by means of a suitable valve.

Choice in arrangement of the three support frames, the several rotor and spring sizes available, range in dashpot stiffness and choice of rotor position on the shaft afford a broad selection of configurations possible of investigation with this test rig.

3.2 Test Configuration and Major Components

3.2.1 Drive Disk and the Bearing and Linkage Complex

Drawings of these components are shown in Appendix A. Pertinent properties are listed in Table I, Physical Properties of Components. Figure 2 shows the drive assembly and Fig. 3, the bearing and linkage complex.

3.2.2 Springs

Figure 3 shows springs mounted in support of one of the shaft bearings. Details of the various springs are shown in Appendix A and listed in Table I.

Spring constants were calculated by formula, [6].

P = load, lbs.
F = deflection caused by given load, in.
G = shear modulus, lbs./sq. in.
d = wire diameter, in.
D = mean diameter of spring, in.
N = number of effective working coils

$$\frac{P}{F} = \frac{G\ d^4}{8\ N\ D^3} \text{ lbs./in.}$$

Table I

PHYSICAL PROPERTIES OF COMPONENTS

Component	Mat'l	L(in)	D(in.)	t(in.)	$I^{\#}_{dia.}$ ($in.^4$)	W(lb.)	M(m.u.)*
Drive disk	Al		7.5	0.5		2.035	0.00527
Bearing Ass'y							
Piston	St'l					2.32	
Conn. bushing	St'l					0.38	
Top pin	St'l					0.25	
Hold tights(2)	St'l					0.83	
Lower pin, ring, ring links(2), bearing	St'l					4.10	
Assembly - total						7.88	0.02041
Shaft	St'l	48	0.5		0.00307	2.61	0.00676
Rotor + rim wt.	St'l		6.0	1.5		14.48	0.03751

$^{\#}I_{dia.}$ = Diametral moment of inertia = $\frac{\pi D^4}{64}$ $in.^4$

$^{*}M(m.u.) = \frac{W}{g} = \frac{W}{386}$ (lb. $sec.^2$/in.)

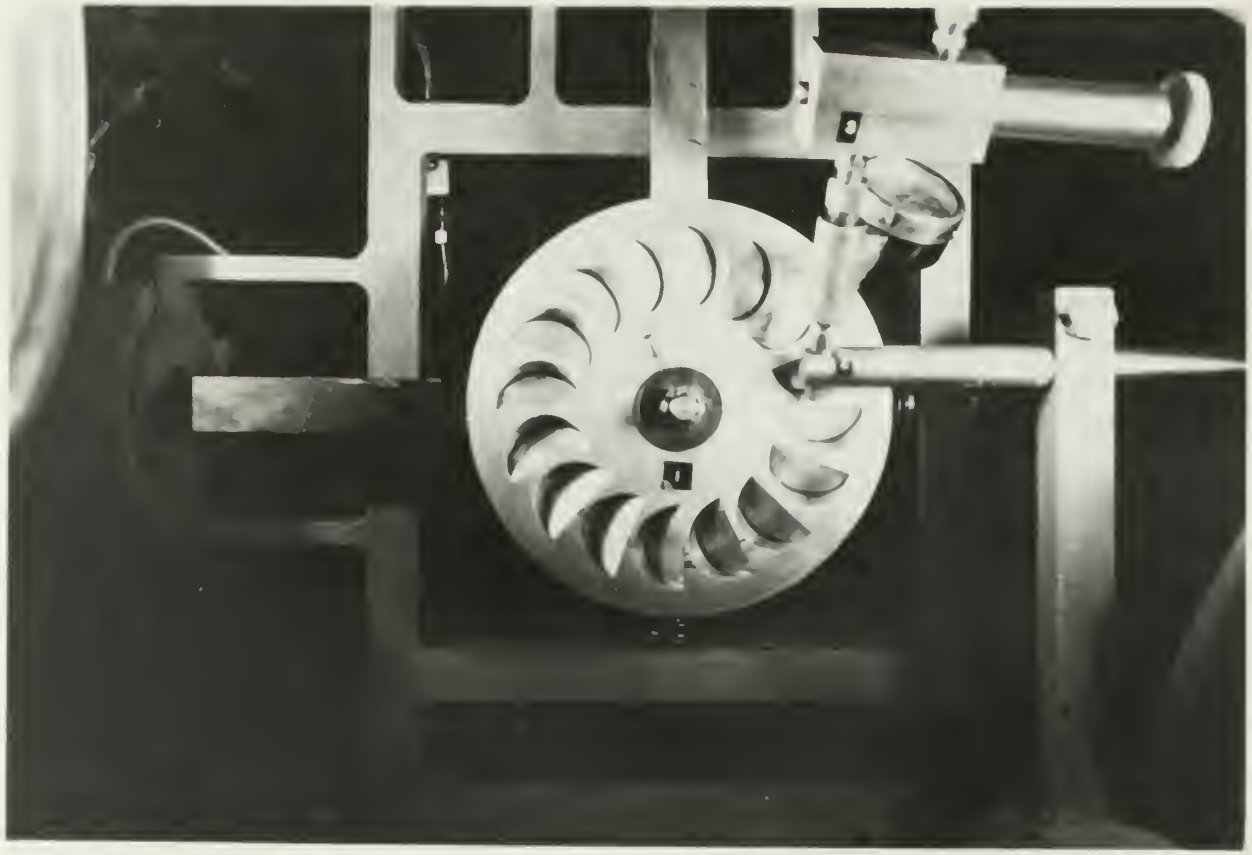

Figure 2 Drive Assembly

1. Cusped, aluminum drive disk
2. Compressed air nozzle
3. Control valve

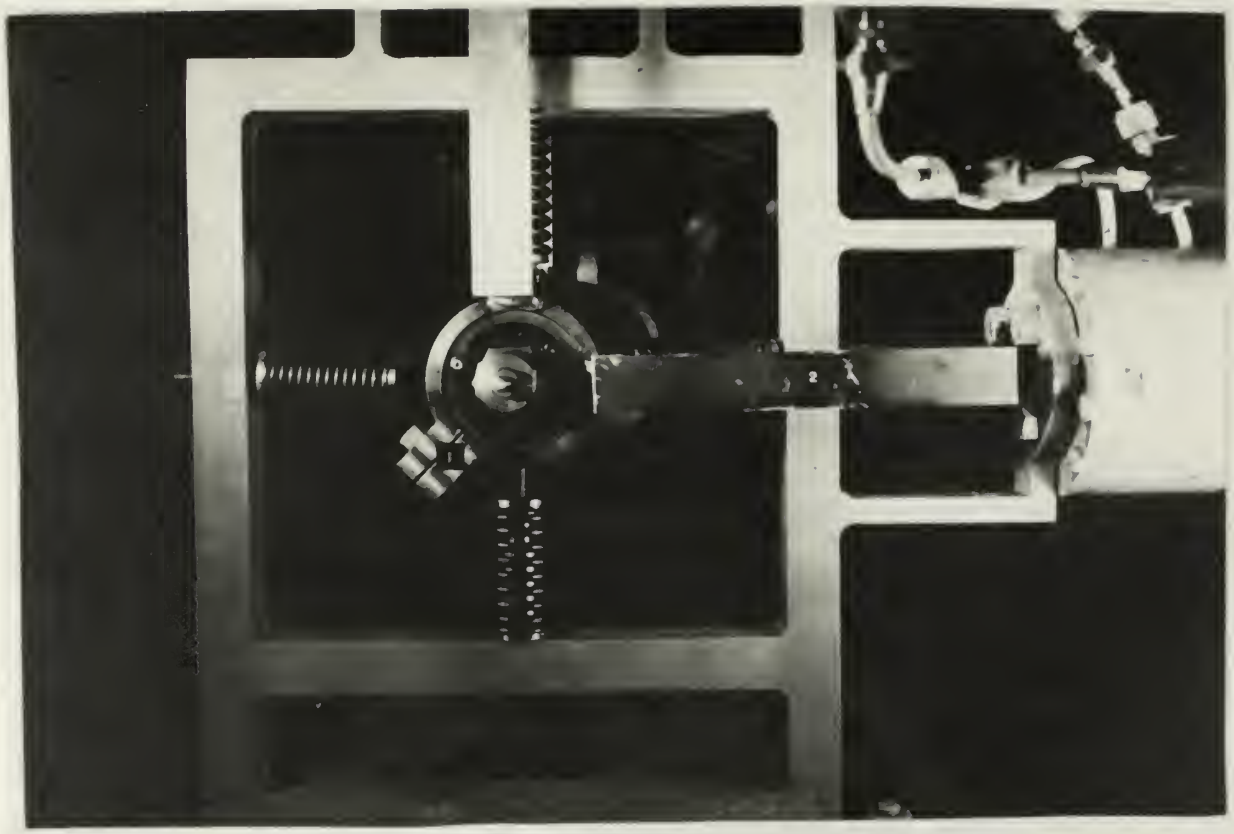

Figure 3 Bearing and Linkage Complex

1. Bearing ring
2. Linkage to dashpot

Light Spring

$$\frac{P}{F} = \frac{11.4 \times 10^{6} \times 2.07 \times 10^{-4}}{8 \times 12 \times 1.4} = 17.5 \text{ lbs./in.}$$

Intermediate Spring

$$\frac{P}{F} = \frac{11.4 \times 10^{6} \times 9.82 \times 10^{-4}}{8 \times 8 \times 1.63} = 107 \text{ lbs./in.}$$

Spring constants were also determined experimentally. The spring and its holder were set vertically over a slot in a fixed surface. A small wire attached to the top holder was led along the axis of the spring and through the slot in the table. The unloaded length of the spring was measured with a vernier caliper. Weights of known sizes were attached to the free end of the wire. The length of the spring was measured for each increment of step-wise loading, and similarly during unloading. Results are listed in Table II, Calibration of Light and Intermediate Springs. Results are shown graphically in Figs. 4 and 5 for light and intermediate spring respectively. Calculated and measured values of spring constants are listed in Table III, Measured and Calculated Spring Constants, for purposes of comparison.

The lack of agreement in the calculated and test values for the light spring indicates that friction in the holders may have had a strong influence on the experimental results. Further testing of the spring is advisable. Both Fig. 4 and 5 show pronounced hysteresis losses are present during compression and relaxation of the springs. The slopes of the figures, from which the response was calculated, were not strongly effected by hysteresis. The experimental value of the intermediate spring constant, in good agreement with the calculated value, was used in all subsequent calculations. Only the intermediate spring was used in tests for critical speeds.

Table II

CALIBRATION OF LIGHT AND INTERMEDIATE SPRINGS

LIGHT SPRING		INTERMEDIATE SPRINGS	
Wt.(lbs.)	Deflection(in.)	Wt.(lbs.)	Deflection(in.)
0.0	0.0	0.0	0.0
1.0	0.053	1.0	0.061
2.0	0.062	2.0	0.109
3.0	0.066	3.0	0.152
4.0	0.078	4.0	0.238
5.0	0.083	5.0	0.290
6.0	0.091	6.0	0.382
7.0	0.121	7.0	0.513
8.0	0.135	8.0	0.597
9.0	0.146	7.0	0.550
10.0	0.168	6.0	0.506
9.0	0.149	5.0	0.447
8.0	0.143	4.0	0.365
7.0	0.133	3.0	0.281
6.0	0.122	2.0	0.214
5.0	0.110	1.0	0.142
4.0	0.101	0.0	0.101
3.0	0.087		
2.0	0.082		
1.0	0.070		
0.0	0.062		

Figure 5

Intermediate Spring Experimental Calibration Curve

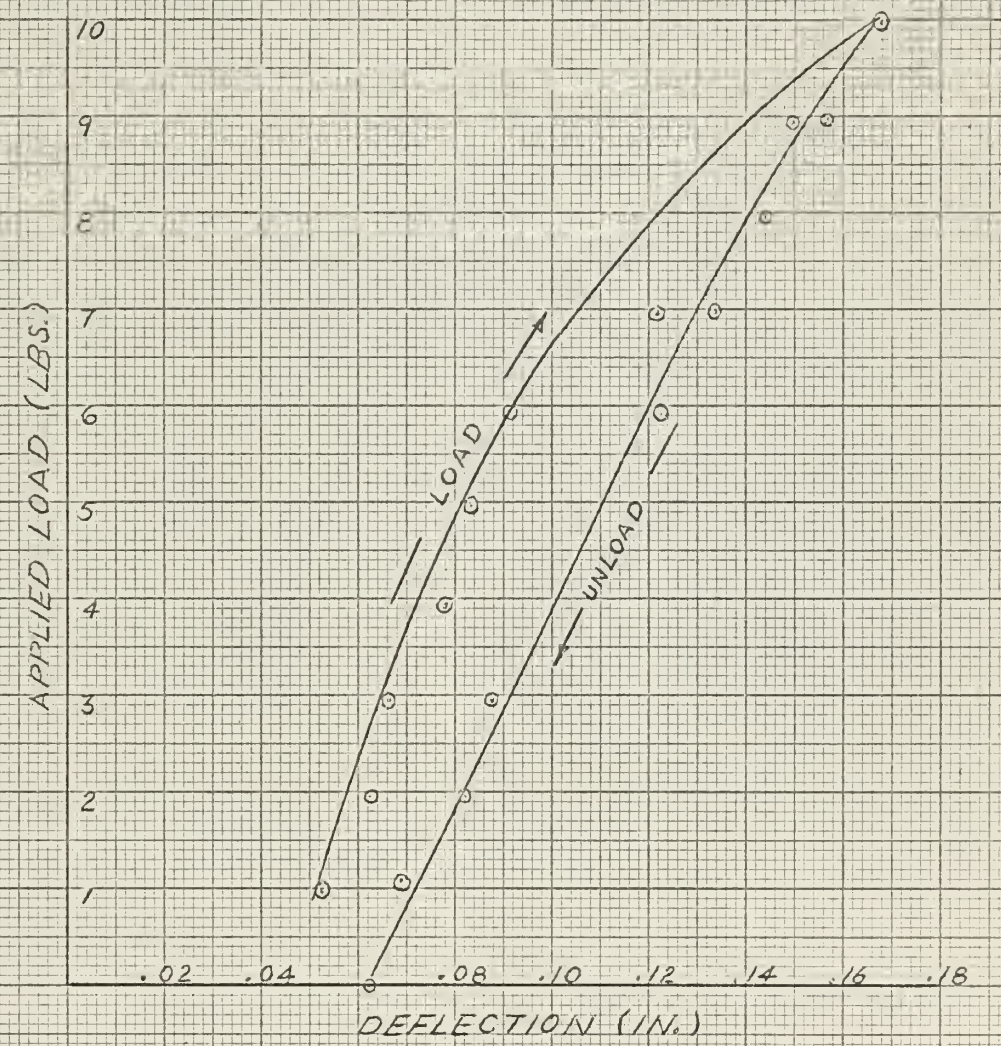

Figure 5

Intermediate Spring Experiment 1 Calibration Curve

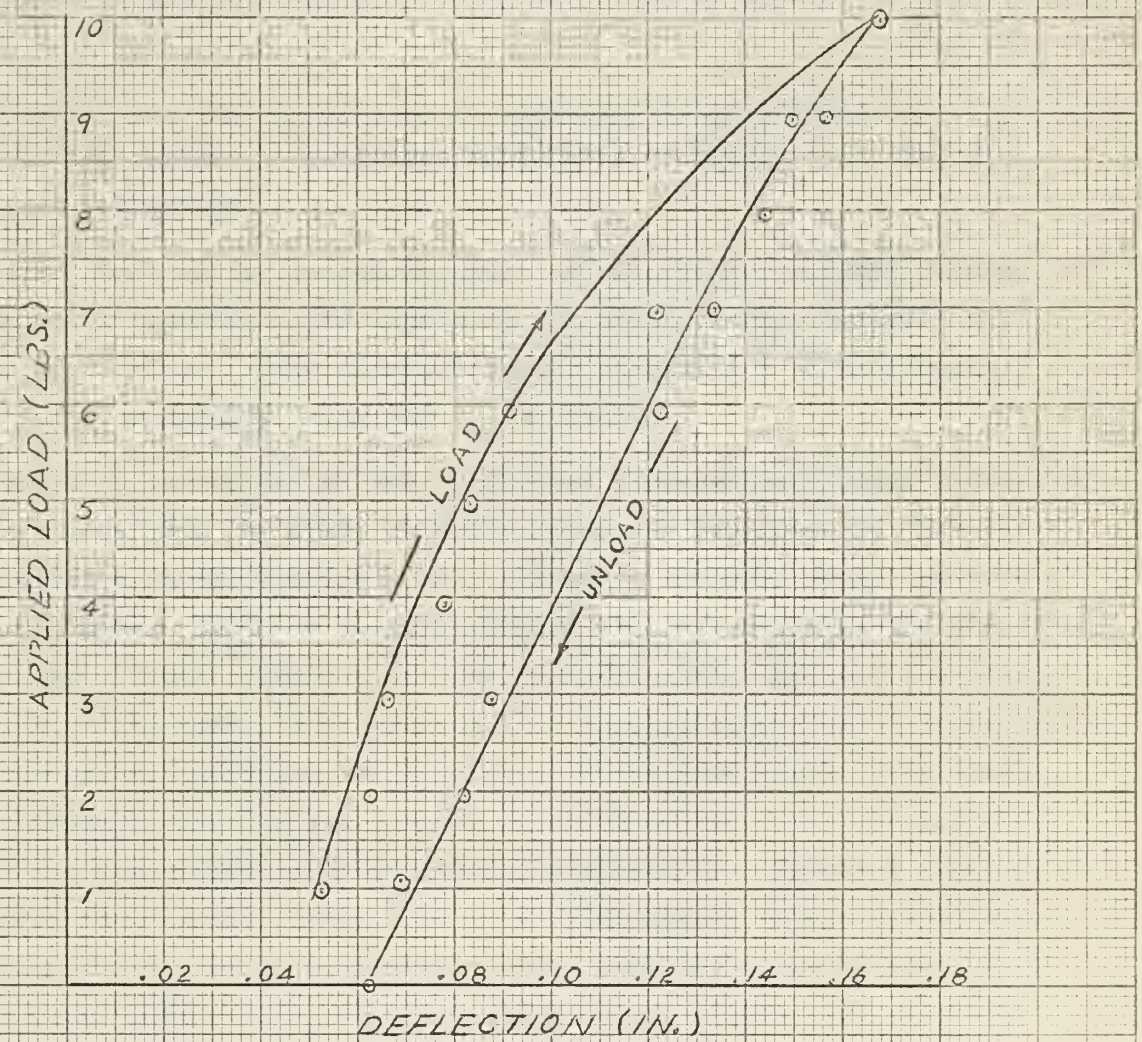

Table III

MEASURED AND CALCULATED SPRING CONSTANTS

Spring	Measured Constant	Calculated Constant	% Variation*
Light	14.5	17.5	20.5
Intermediate	105.5	107.0	1.4

*based on measured value

3.2.3 Shaft

Dimensions and physical properties are shown in Appendix A and Table I.

The shaft was checked for set or eccentricity by rolling on a precision flat surface. Variations noted were so slight that they did not warrant correction.

Static shaft spring properties were calculated for midspan loading with pin-ended supports. The length of the shaft between supports was taken as 40.5 inches. From elementary beam theory, $K = 48\ EI/(\text{length})^3$ lbs./in. The calculated value was 65.33 lbs./in.

The spring properties of the shaft were also evaluated experimentally. Tests were made with the shaft on knife-edged end supports and with the shaft supported in the bearings. Any change in response would indicate a resisting moment could be exerted despite the self-aligning feature of the bearings. Tests were made for the unloaded shaft and with the rotor in position at midspan. With the shaft on supports placed 40.5 inches apart loading and unloading was conducted in the same manner described for the springs. Results are listed in Tables IV and V for the knife-edge and bearing support end conditions respectively. Figure 6 shows the experimental results graphically. No significant change resulted from the change in end support conditions. From the slope of the curve in Fig. 6 the shaft stiffness was calculated as 66.5 lbs./in. Although the test with the bearing showed some hysteresis loss the effect was small, and was therefore disregarded. The experimental value, in close agreement with the theoretical value, was used in all subsequent calculations.

Table IV

STATIC SHAFT SPRING CALIBRATION - KNIFE EDGE SUPPORTS

Wt.(lbs.)	Deflection(in.)	*W_{rotor} Wt.(lbs.)	Deflection(in.)
0.0	0.0	W_r +0.0	0.0
1.0	0.014	+1.0	0.016
2.0	0.029	+2.0	0.032
3.0	0.042	+3.0	0.046
4.0	0.057	+4.0	0.064
5.0	0.072	+5.0	0.080
6.0	0.088	+6.0	0.090
7.0	0.103	+7.0	0.107
8.0	0.116	+6.0	0.093
9.0	0.132	+5.0	0.079
10.0	0.146	+4.0	0.064
11.0	0.160	+3.0	0.048
12.0	0.178	+2.0	0.032
11.0	0.164	+1.0	0.016
10.0	0.147	W_r +0.0	0.003
9.0	0.132		
8.0	0.117		
7.0	0.102		
6.0	0.086		
5.0	0.072		
4.0	0.056		
3.0	0.042		
2.0	0.029		
1.0	0.014		
0.0	0.0		

*W_r = 14.5 lbs.

Table V

STATIC SHAFT SPRING CALIBRATION - BEARING SUPPORTS

Wt. (lbs.)	Deflection(in.)	$*W_{rotor}$ Wt.(lbs.)	Deflection(in.)
0.0	0.0	W_r +0.0	0.0
1.0	0.015	+1.0	0.019
2.0	0.028	+2.0	0.041
3.0	0.041	+3.0	0.050
4.0	0.061	+4.0	0.070
5.0	0.076	+5.0	0.084
6.0	0.091	+6.0	0.103
7.0	0.108	+7.0	0.115
8.0	0.125	+6.0	0.103
9.0	0.145	+5.0	0.090
10.0	0.157	+4.0	0.074
11.0	0.172	+3.0	0.060
12.0	0.190	+2.0	0.046
11.0	0.181	+1.0	0.030
10.0	0.164	W_r +0.0	0.014
9.0	0.149		
8.0	0.135		
7.0	0.121		
6.0	0.103		
5.0	0.088		
4.0	0.076		
3.0	0.055		
2.0	0.042		
1.0	0.029		
0.0	0.016		

$*W_r$ = 14.5 lbs.

Figure 6

Shaft Spring Constant Experimental Calibration Curve

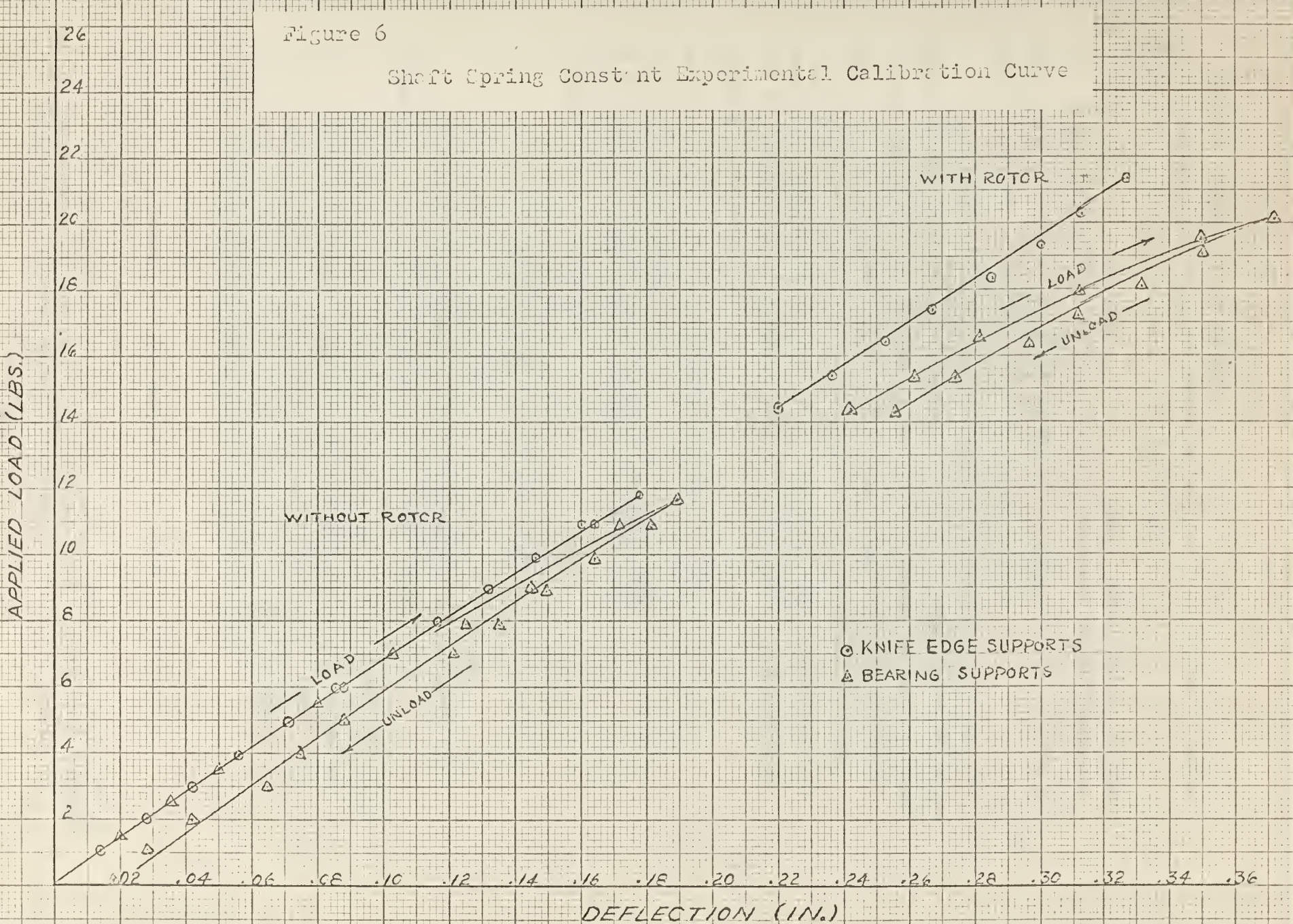

3.2.4 Rotor and Lip Weight

Details of the rotor are shown in Appendix A and listed in Table I. Figure 7 shows the relative size of these parts.

The rotor was balanced statically. Dynamic balancing was considered, but it was felt that the disk, only 1.5 inches thick, would produce only small effects due to possible variations in properties between its parallel planes.

The rim weight, which was introduced after static balancing, was employed for two purposes. Knowledge of its size permitted calculation of rotor eccentricity, defined as the shift in center of gravity of the rotor due to the added weight. This value is essential to accurate calculation of exciting forces developed during rotation. Secondly, considering the aforementioned static balancing, the imbalance due to the lip weight would overshadow effects of any small variations not removed in the balancing.

The eccentricity was calculated as follows:

W = basic rotor weight, lbs.
w = added rim weight, 0 04 lbs @ 2.75 in. from axis
$\bar{x}$ = location of displaced c.g. from polar axis, in.

Moment about $\bar{x} = W\,\bar{x} - w(2.75 - \bar{x}) = 0$

$$\bar{x} = \frac{0.04 \times 2.75}{14.44 + 0.04} = 0.0076 \text{ in.} = \epsilon$$

3.2.5 Control System

Details of the components of the control system are shown in Appendix A. The general arrangement is shown in Fig. 2.

The item referred to as the control valve in Fig. 2 was not designed specifically for this use. It is identical to the needle valves used as metering devices for the working fluid in the dashpots. Large adjustments in supply of compressed air to the drive jet were made by means of a coarse valve in the line upstream of the control valve.

3.2.6 Dashpots

Detailed drawings of the dashpots are shown in Appendix A.

Smith, [7], has written,

> The assumption as to the viscous law of damping is not fulfilled in practice and analytical predictions as to the effect of damping are, to some degree, only qualitative.

Figure 7 Rotor and Lip Weight

The dashpots required extensive testing to determine their characteristics. It was desired to determine three main factors: (1) the degree to which the dashpots were linear, (2) the dependence of the magnitude of damping on the direct communication port openings (See Fig. 8), and (3) the range of damping "constants" possible within limits of needle valve settings.

Any attempt to evaluate the dashpots by analysis of the internal flow would require numerous assumptions. An analytical description of the non-steady flows through the bypass tubing and direct communication ports would have resulted in a doubtful approximation at best.

A method based on direct measurement of drive force, acceleration and velocity response was used.

3.2.6.1 Instrumentation and Test of Dashpots

A dashpot was mounted on a fixed platform above a Ling Electronics Model 219 Shaker as shown in Fig. 9. A drive spindle of 6061-T6 aluminum, {8}, was made to accept the male thread of the dashpot piston shaft. The spindle, except for the end portions, was square in cross section. The width of the sides of the cross section was machined to 0.250 ± 0.001 inches. Two SR-4, type A-7 strain gages, {9}, were mounted axially on opposite sides of the spindle. The gages were connected in series to increase sensitivity to strain, and at the midpoint of the spindle to avoid effects from the non-uniform ends. The other end of the spindle was threaded into an adaptor on the drive table of the shaker.

Two accelerometers were mounted on the adaptor. Figures 10 and 11 illustrate the details of the arrangement. A Statham Model 5A5-100-120 accelerometer was used to measure accelerations. Its output, as well as that from the strain gages, was led to the Honeywell Model 130-2C Carrier Amplifier shown as item 7 in Fig. 12. Both amplified signals were recorded semi-permanently on the output paper of the Heiland Model 906B Oscillograph Visicorder, item 6, Fig. 12. An electronic timer imposed time reference lines on the simultaneous trace of acceleration and strain. The output of the second accelerometer, a Consolidated Engineering Corporation Model 4-102-A Vibration Pickup, measured

Figure 8 Dashpot Piston

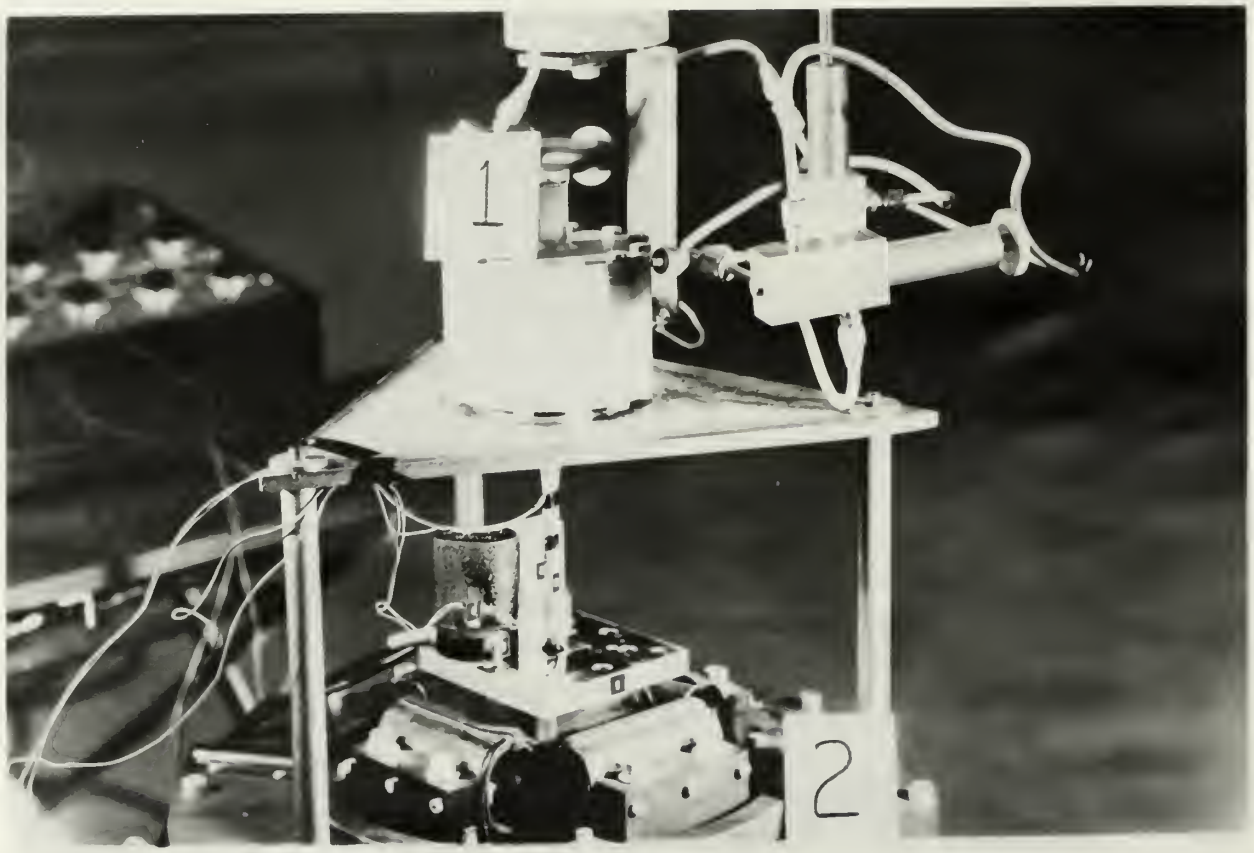

Figure 9 Dashpot - Shaker Test Set Up

1. Dashpot mounting
2. Shaker

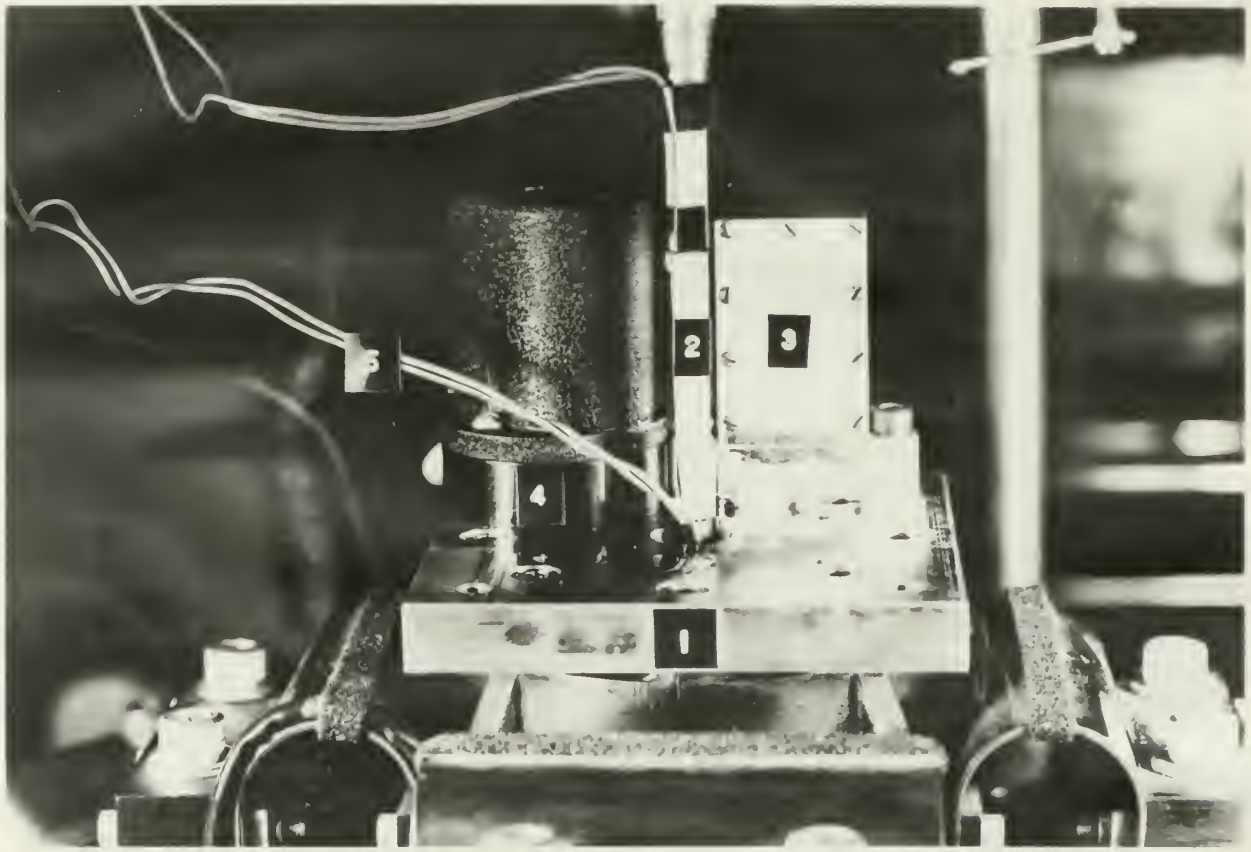

Figure 10 Shaker Drive Table Detail

1. Adaptor table
2. Drive spindle
3. Statham accelerometer
4. Conoflex mod accelerometer
5. Strain gage output leads

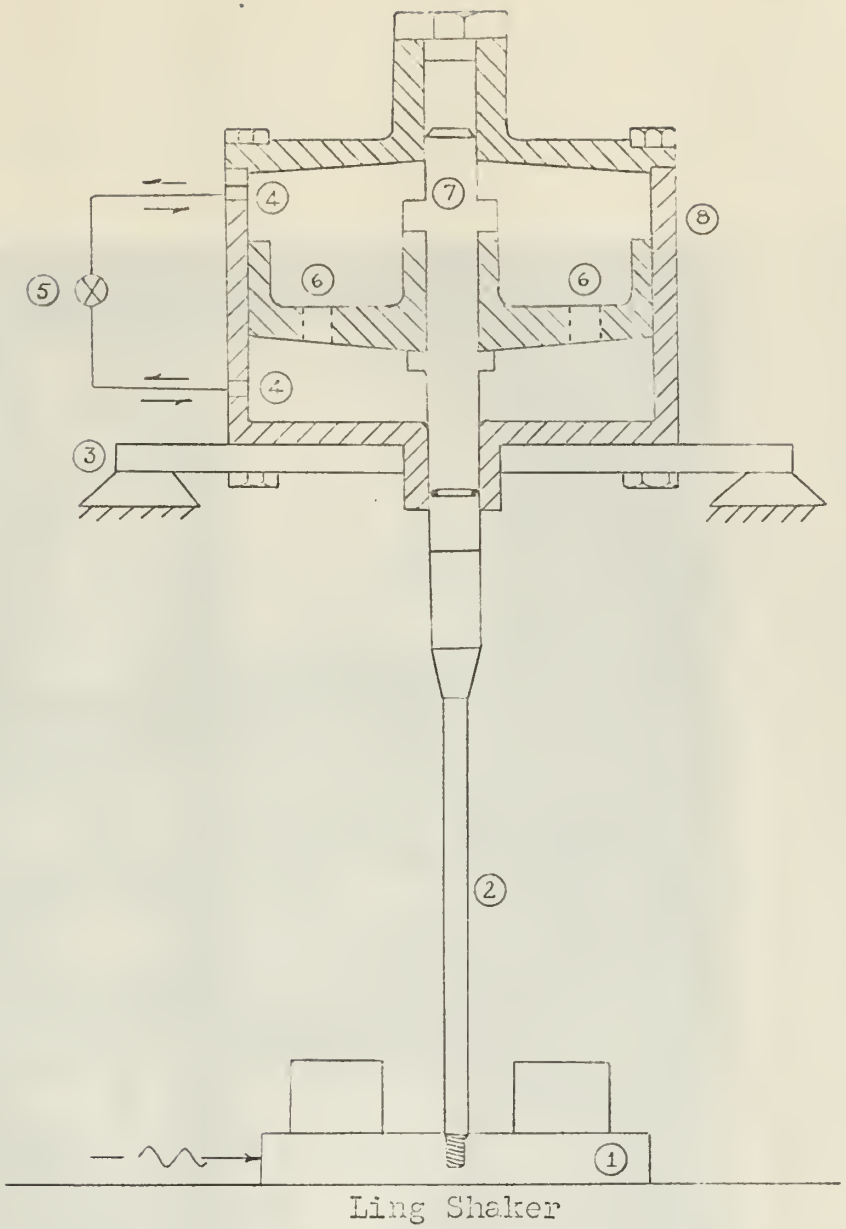

Figure 11 Dashpot Test Configuration

1. Shaker table, accelerometers
2. Aluminum spindle, ¼ x ¼ x 6" with A7 strain gages
3. Fixed, 3/8" steel plate
4. Bypass ports
5. Control valve
6. Communication ports
7. Piston rod
8. Dashpot cylinder

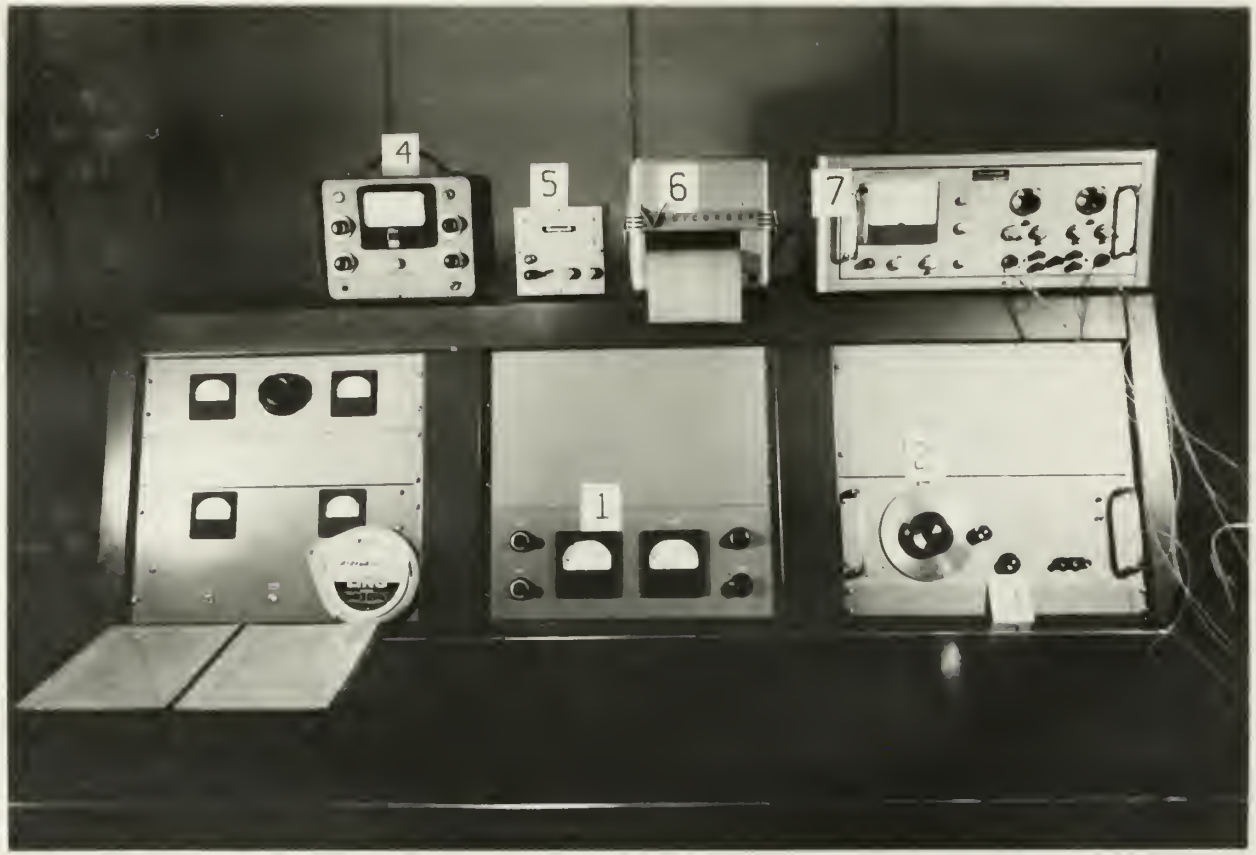

Figure 12 Dashpot Test Console and Instrumentation

1. Shaker control console
2. Frequency control
3. Amplitude control
4. Vibration meter
5. Timer
6. Visicorder
7. Carrier amplifier

velocity and peak-to-peak amplitude of vibrations. Readings of average velocity and displacement were indicated on a Consolidated Electrodynamics Corporation Type 1-117 Vibration meter. The velocity, amplified by the vibration meter, was led to a Hewlitt-Packard Model 120A Oscilloscope. A typical trace of the variation of velocity with time is shown in Fig. 13. Operating frequency was read directly from the frequency control dial on the shaker control console.

The strain trace on the Visicorder was calibrated in accordance with operating instructions for the system. The dashpot was charged with H-515 OHA petroleum base hydraulic fluid, {10}. Several combinations of port openings and bypass valve settings were observed. Operation with hydraulic fluid in the dashpots was conducted in some cases and air was used in other instances.

It was believed that even the minimum possible damping on the part of the dashpots might prove excessive in relation to other characteristics of the system. It was decided to attempt to approximate the case of zero damping.

The dashpot configuration which would produce minimum damping obviously required the bypass line and communication ports to be unrestricted. The only question lay in the choice between air and hydraulic oil as the working fluid. Although the choice of air would seem the more logical, there was a higher likelihood of large frictional forces associated with its use. It is not known whether an air loaded dashpot would, in fact, produce less damping than that which was measured, but the hydraulic fluid was selected for use in the test based on its lubricating properties.

The plugs were removed from the communication ports and the bypass valve was set fully open. Average velocity for the test was 3.0 in./sec. Peak-to-peak displacement was 0.28 in. at the test frequency of 5 cps.

Traces of acceleration and strain (force) were scaled up four-to-one for readability. Figure 14 shows only the basic variations of force and accelerations as recorded on the trace. Superimposed on the actual trace was a high frequency "hash". This was present during the warm up

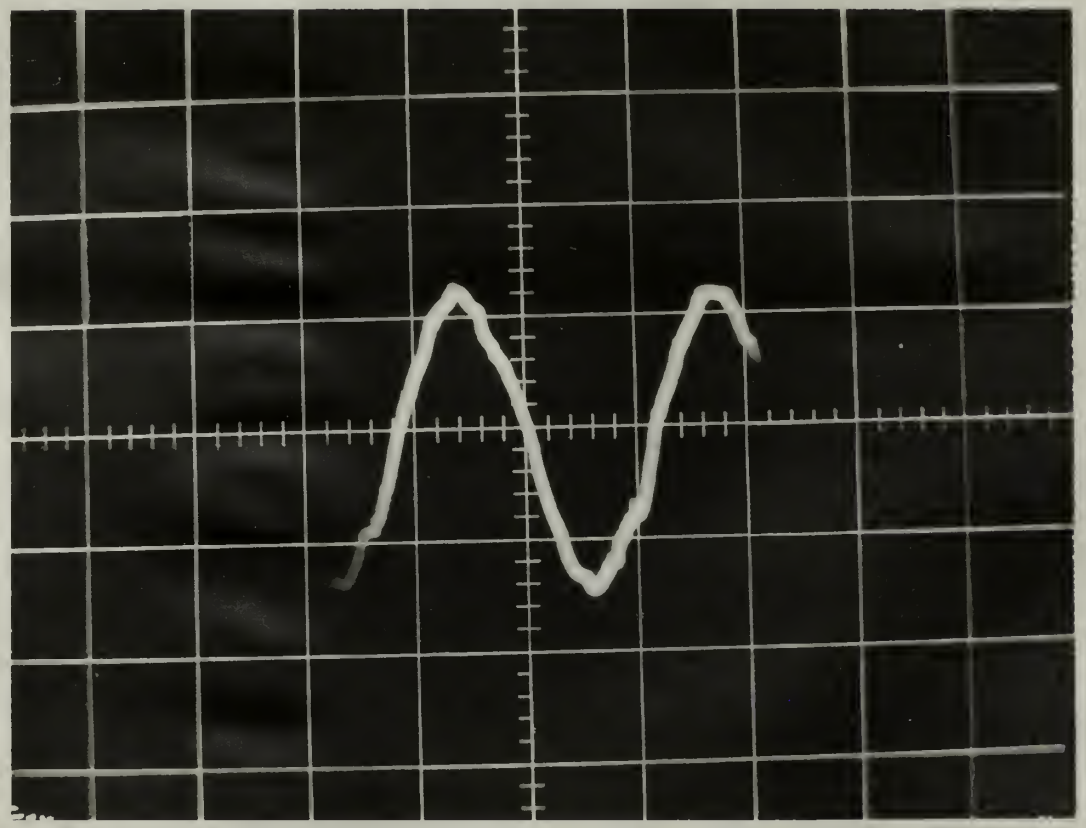

Figure 13 Piston Velocity Trace

Figure 14

Dashpot Test Responses

a. Acceleration vs. Time
b. Velocity vs. Time
c. Displacement vs. Time
d. Force vs. Time

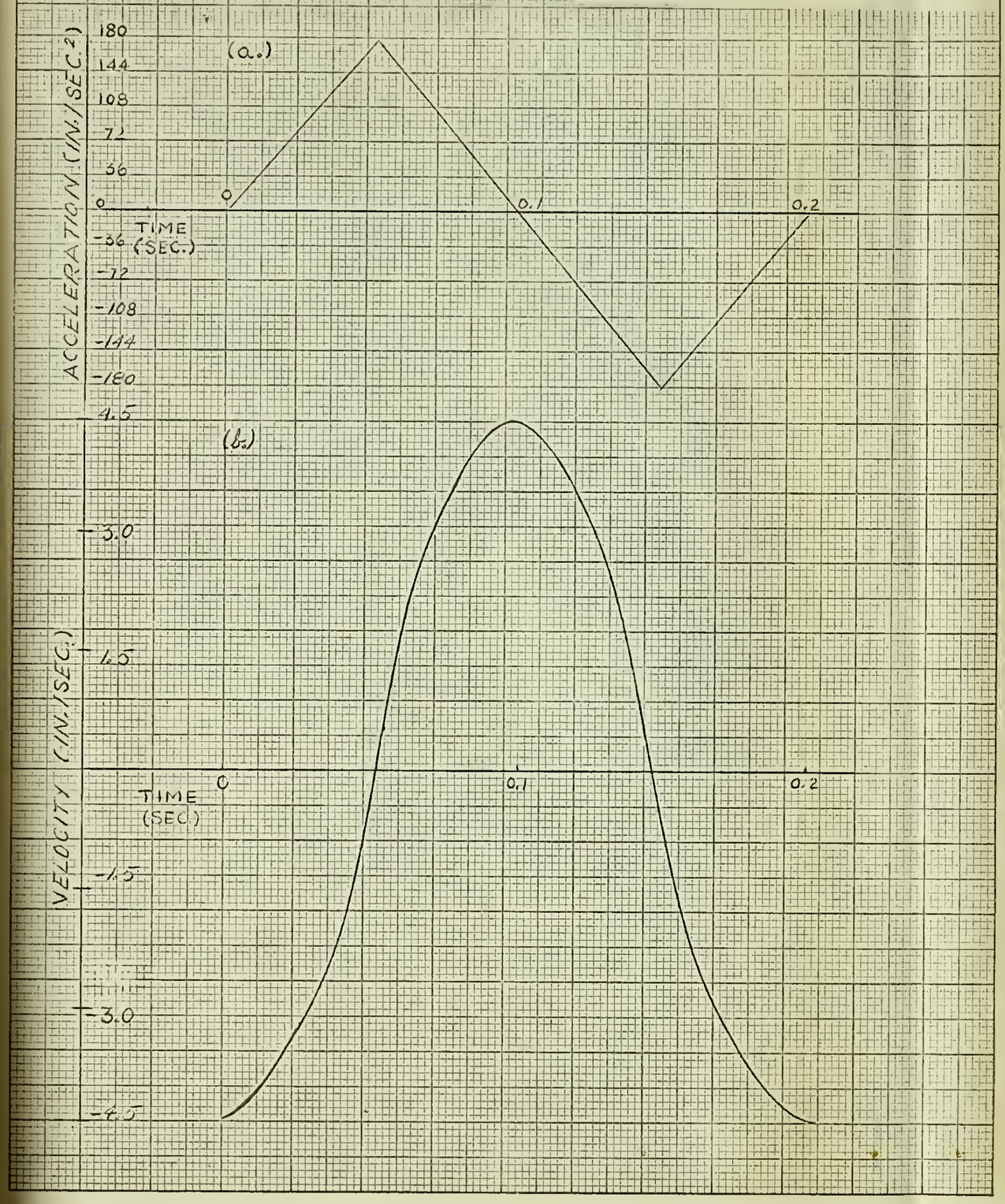

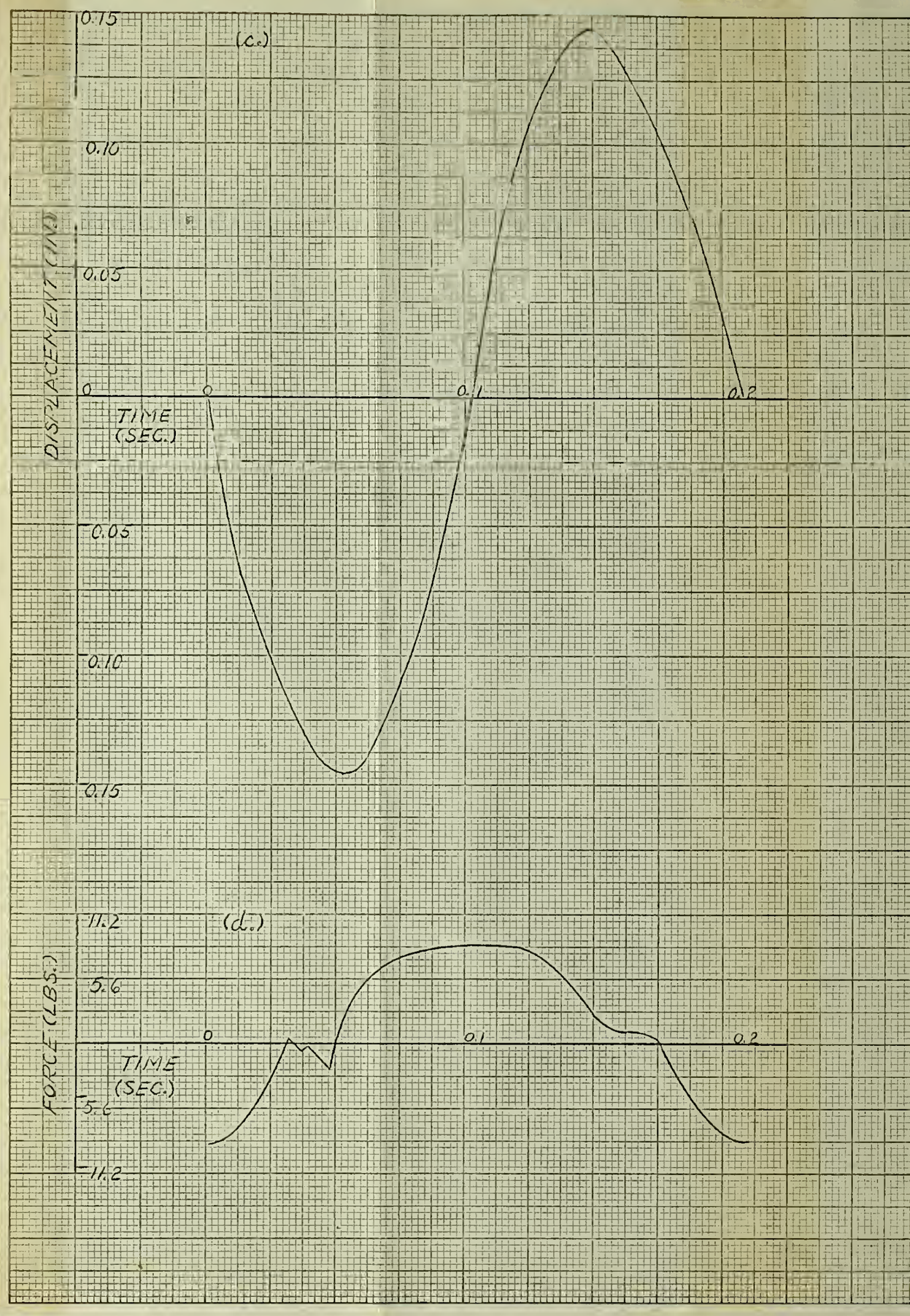

of the shaker prior to actual tests. Since these signals were obviously not associated with response of the dashpot they were disregarded in the interpretation of the test traces. By successive integrations of the acceleration trace, velocity and displacement traces were produced. These waveforms are shown in Fig. 14 a-c. The associated force trace is shown in Fig. 14 d. Integration of the acceleration wave produced a parabolic velocity trace. The velocity trace was scaled from the known value of the average velocity, two-thirds of the maximum velocity representing the average height of the parabolic trace. The scale of the acceleration trace was found from the fact that the area under the acceleration curve was equal to the known maximum velocity.

According to design specifications the shaker should have produced a sinusoidal output with maximum of 3 percent distortion at 5 cps. The derived displacement-time relationship was not a sine wave. Whether this was due to instrumentation error or to shaker operation with distortion greater than that cited in the specifications is not known.

With the assumption of sinusoidal motion for the system depicted in Fig. 15 the following relationships apply:

F_I = inertia force = $m\ddot{x}$; F_d = damping force = $c\dot{x}$

F_T = total force = $F_I + F_d$

$x = A \sin \omega t$, $\dot{x} = \omega A \cos \omega t$, $\ddot{x} = -\omega^2 A \sin \omega t$

$$\sin \omega t = \frac{x}{A} = \sqrt{1 - \left(\frac{\dot{x}}{A}\right)^2} \qquad \cos \omega t = \frac{\dot{x}}{\omega A} = \sqrt{1 - \left(\frac{x}{A}\right)^2}$$

$$F_I = -m\omega^2 A \sqrt{1 - \left(\frac{\dot{x}}{A}\right)^2} \quad \therefore \quad \left[\frac{F_I}{-m\omega^2 A}\right]^2 + \left(\frac{\dot{x}}{\omega A}\right)^2 = 1 \text{, AN ELLIPSE}$$

$F_d = c\dot{x}$, a straight line whose slope is c.

$F_I = -m\omega^2 x$, a straight line whose slope is $-m\omega^2$.

$$F_d = \omega c A \sqrt{1 - \left(\frac{x}{A}\right)^2} \quad \therefore \quad \left[\frac{F_d}{\omega c A}\right]^2 + \left(\frac{x}{A}\right)^2 = 1 \text{ , AN ELLIPSE}$$

Figure 15

. Ideal Graphic Relationships

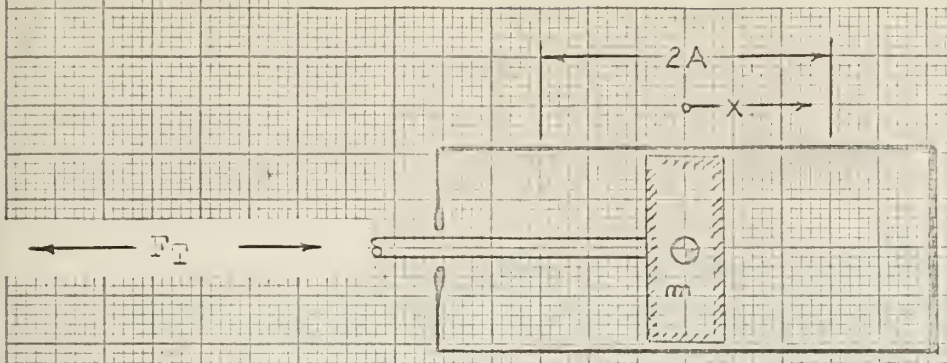

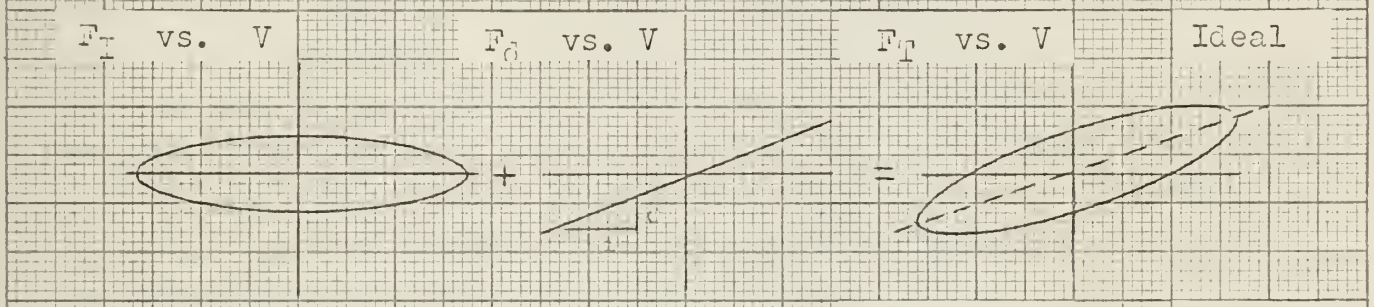

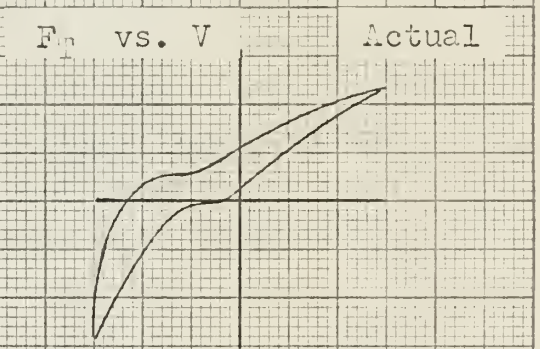

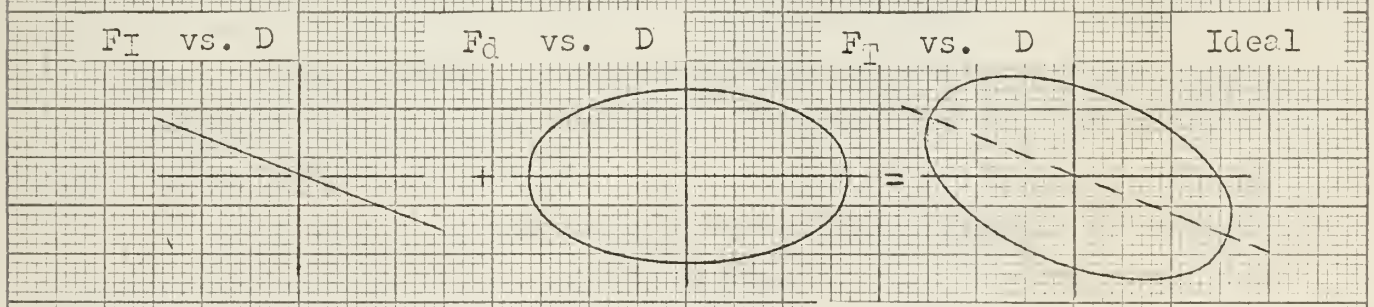

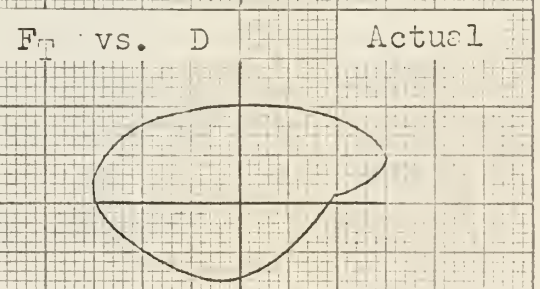

Figure 15 shows these relationships graphically. The ellipse in the velocity plot has a minor semi-axis proportional to the inertia or mass of the system. The minor semi-axis of the displacement plot is proportional to the force of viscous damping in the system. Representative plots of experimental data are included for purposes of comparison.

Consistent with the nature of the forces involved the inertia force contributes nothing to the area of the displacement plot.

Test data plotted in Fig. 16 indicate the variation of total force with velocity. The shape of the enclosed area differs markedly from the ideal form of an ellipse. The distortion of the figure emphasizes the remarks cited at the beginning of this section. The non-linearity is strongest in the region of negative velocity. Deviation from the ideal case is also apparent in the recorded force trace, Fig. 14 d. This may have been caused by coverage of the bypass ports at the extreme point of the piston stroke, by large friction forces present due to momentary loss of lubrication between the dashpot cylinder and the piston surfaces, or by lag in the mechanical linkage between the drive table and the piston. The vertical offset of the center of the closed figure from the origin indicates that the force is dependent to some degree on the absolute direction of motion. No logical reason for such a dependence is apparent.

For a linear system the slope of the mean line of the F_T - velocity plot is equal to the damping constant. Since no dependable mean line is apparent, the slope of a line drawn through the endpoints of the figure is considered only as a first estimate. The slope so defined was calculated as 1.88 lbs./(in./sec.)

In an attempt to analyze the F_T - velocity trace further, the product of mass and acceleration was subtracted point-by-point from the total force ordinate. Figure 17 shows the result as a "Reduced Force"-velocity plot. A further refinement of this figure could be made by an allowance for the mass of fluid being accelerated during the operation of the dashpot. Regardless of the distortions in Figs. 16 and 17 it can be said that, essentially, the dashpot response has been established.

Figure 16

Dashpot Test, Force vs. Velocity

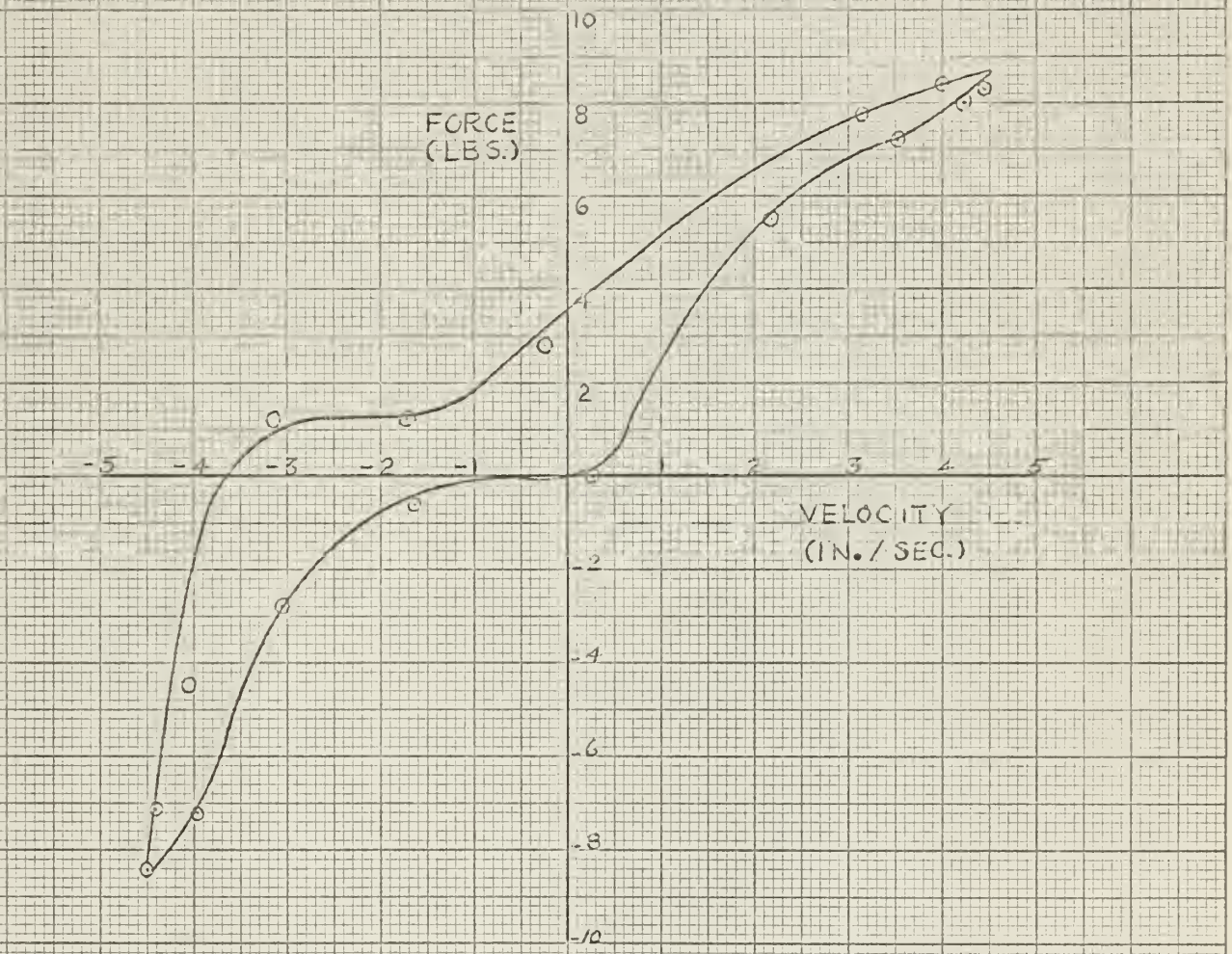

Figure 17

Desired Test, "Reduced Force" vs. Velocity

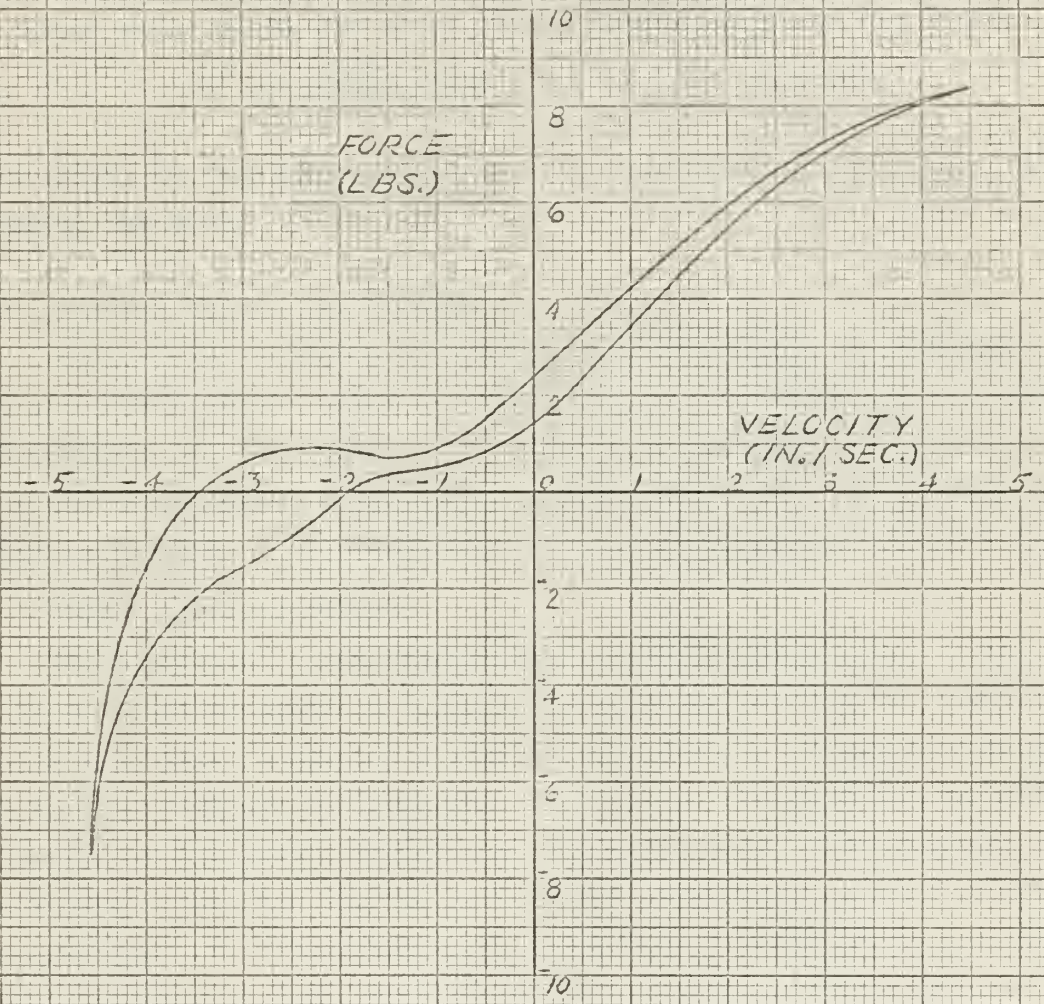

The force-displacement plot from test data is shown in Fig. 18. The closed curve has some resemblance to an ellipse. Assuming that an equivalent damping system will absorb or dissipate equal energy per cycle as does the physical system, an equal area ellipse was constructed. One semi-axis was defined by the known displacement. From the formula for the area of an ellipse, Area = π x a x b, the regular ellipse, shown dashed in the figure, was drawn and superimposed. From the scale of the test figure the semi-axis proportional to $c\omega A$ was measured. Dividing by the known value of ωA the value of the damping constant was found.

$$c = \frac{7.8}{5 \times 6.28 \times 0.14} = 1.77 \text{ lbs./(in./sec.)}$$

This value, in fair agreement with that calculated from Fig. 16, is probably the better of the two.

3.3 Critical Speed Test Program

Tests of the rotating system were conducted with the bearings locked and with the bearings under the restraint of the dashpot-spring combination. The dashpots for the latter test were set in the same configuration used in their calibration, i.e., direct communication ports and bypass control valve fully open. The intermediate spring was employed with the dashpot.

3.3.1 Instrumentation

The electrical probe displacement sensor shown in Fig. 19 was used to measure deflections. A conducting probe in the form of a small spring was fixed to the end of the vernier shank. The vernier micrometer was mounted rigidly in a support. A 22.5 volt dry cell battery provided potential to the probe through the conductor shown. This voltage was impressed in parallel across the vertical deflection circuit of the 120A Oscilloscope. At each instant of contact between the probe and the rotor the scope circuit was grounded and a vertical spike appeared on the scope. Zero readings of the vernier were made prior to each test. The vernier, readable to 0.001 inches, was then backed off. For each speed at which measurement of vibration amplitude was desired the vernier was advanced until first contact was indicated on the scope. Some arcing at the tip of the probe indicated small errors, estimated at $\pm$ 0.005 in., were inherent to the method.

Figure 13

Dashpot Test, Force vs. Displacement

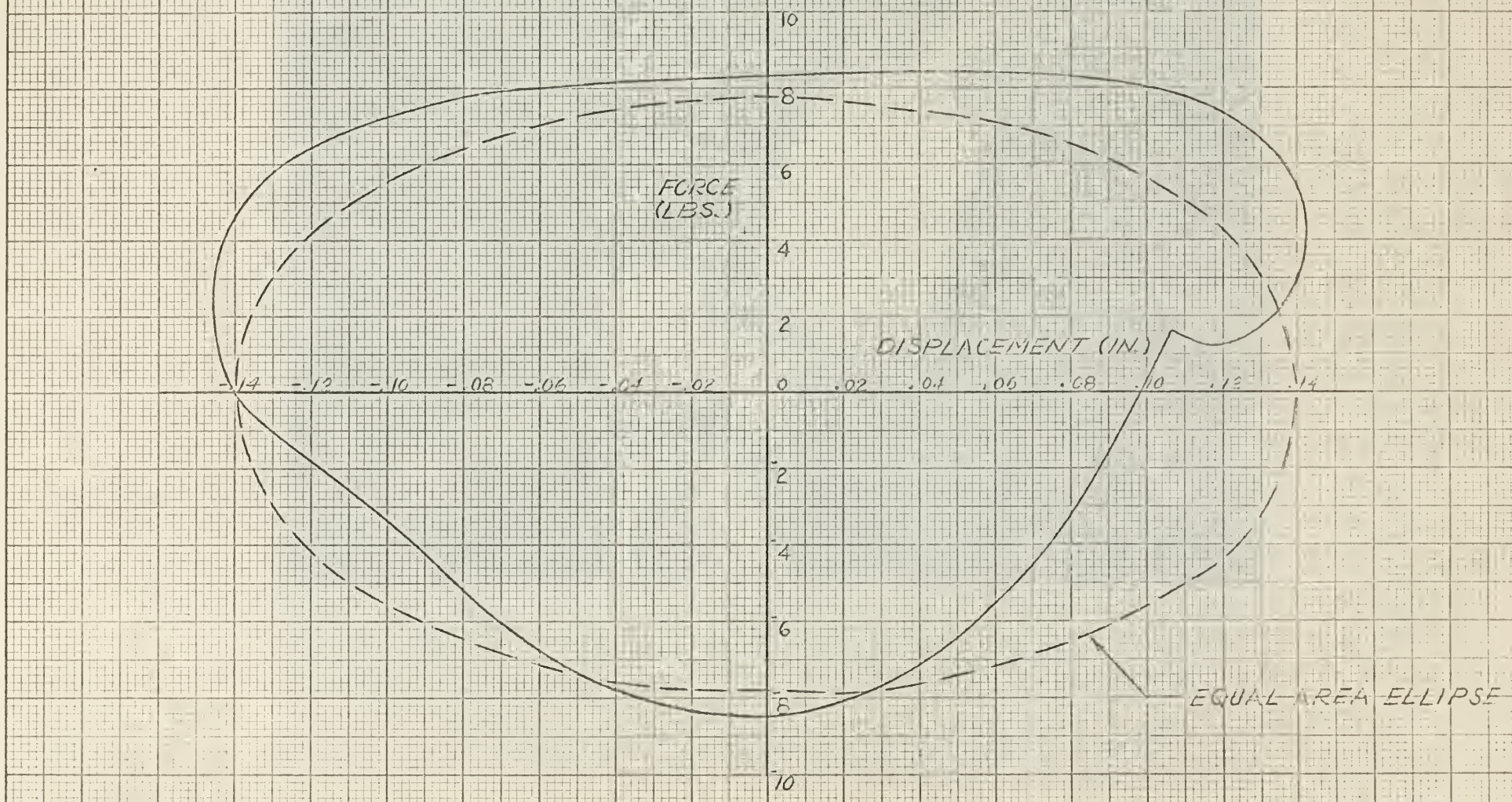

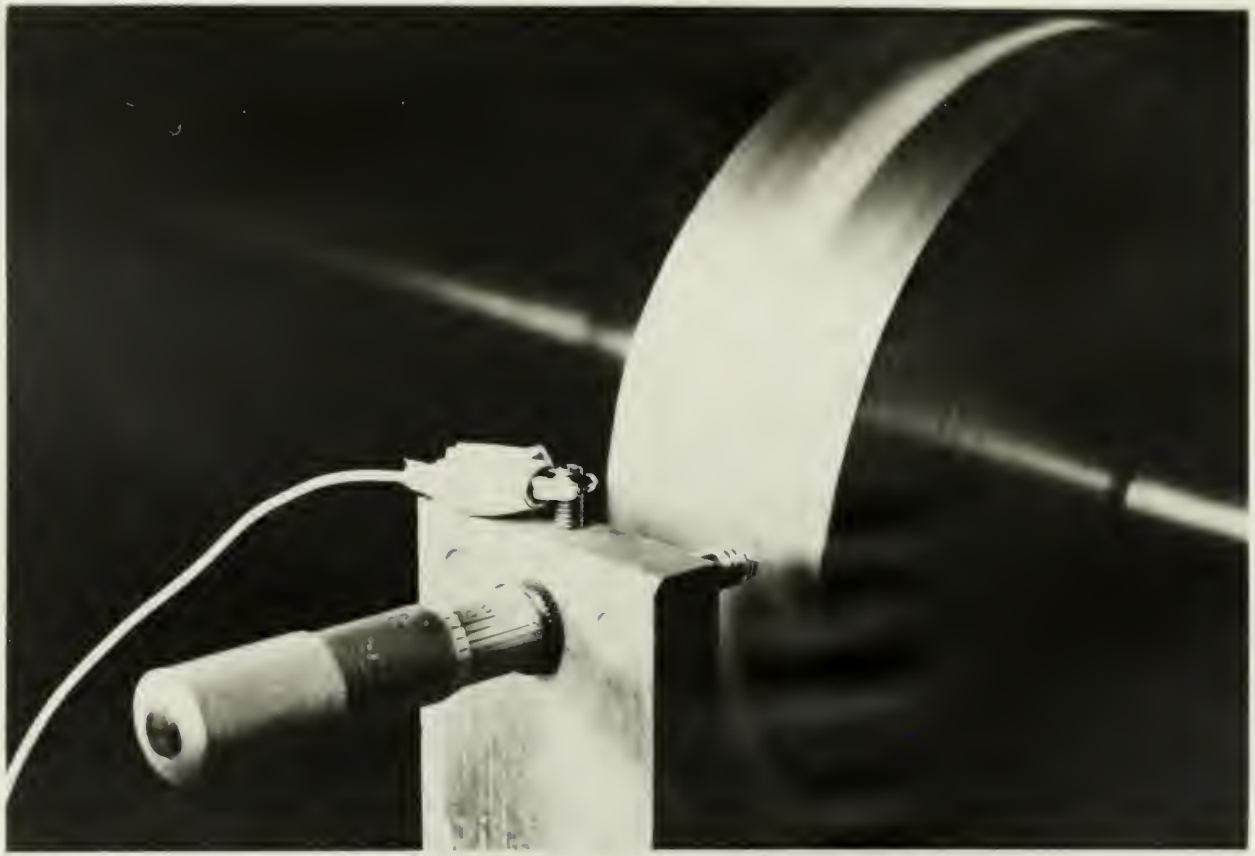

Figure 19 Electric Probe Displacement Sensor

An RCA Model 631B Strobotac was used for speed indications. The low scale on this instrument, usable for speeds from 60 to 3700 RPM, was readable to $\pm$ 2 RPM.

3.3.2 Results

At no time during tests with the bearings supported by the intermediate spring was there any perceptible or measurable motion of the bearings.

Results are listed in Table VI, Experimental Results. Results are shown graphically in Figs. 31 and 39 in conjunction with the comparison of theoretical and experimental results.

3.4 Comments on the Physical System

The system could not be tested without the dashpot linkage, and consequently, the dashpots engaged. This resulted from the inability of the spring-spring holder combination to resist loads normal to its axis. The stabilization provided by the dashpot linkages was desirable in one sense and indicative of a possible source of trouble in another. Forces along the rotor shaft axis were carried through the dashpot linkages to the dashpot pistons. An aggravated case of this could have resulted in the pistons becoming cocked in the dashpot cylinders. Such cocking could have caused deviations from linearity even greater than those observed in the controlled testing of the dashpots.

The light spring was not capable of supporting the combined weight of its associated bearing and the rotor mounted on the shaft. These springs "bottomed" in their holders when the fourteen pound rotor was mounted. A lighter rotor, capable of being supported by the light springs, was mounted. Spring action was linear with the rotor at rest but, movement of the bearings in vibration closed the springs coil-to-coil.

The drive disk whipped noticeably during strong vibration of the system. Air was spilled from the cusps in the disk and a non-steady drive resulted. The disk could be reworked to form channels as in a Pelton type turbine; this would reduce spilling. This same modification would eliminate the small axial component associated with the present drive system.

Table VI

EXPERIMENTAL RESULTS

Bearings fixed	
RPM	Deflection (in.)
250	0.044
260	0.045
270	0.046
280	0.047
290	0.048
300	0.050
310	0.062
320	0.063
330	0.066
340	0.067
350	0.090
360	0.099
370	0.238
372	0.670
375	0.969
380	1.245
385	0.982
390	0.072
395	0.051
400	0.017
450	0 004
500	0.003

Hydraulic fluid in dashpots, bypass and ports open	
RPM	Deflection (in.)
300	0.001
330	0.000
340	0.005
355	0.029
370	0.040
375	0.080
380	0.104
383	0.116
388	0.109
390	0.113
393	0.090
400	0.075
450	0.058

Strong transient vibrations were noted during accelerations of the rotor. The speed control system is not conducive to setting of precise speeds. Low speeds require small inputs from the jet. Acceleration forces must be kept very close to those necessary for steady drive at the speed desired or the speed will build rapidly and overshoot. For low speeds this means allowance for long periods of speed buildup. Fifteen minutes was not excessive for speed stabilization during tests.

Fluctuations in the supply air pressure caused speed to drift even after long periods allowed for stabilization. In consideration of these factors measured speeds can be interpreted as accurate only to within $\pm$ 5 RPM.

Error in the calculation of the dashpot damping constant may have stemmed from either or both of the following: (1) Low amplification of the spindle strain trace such that its maximum value reached only twenty percent of the lowest mark on the calibration scale of the recorder. (2) Reading and scaling of recorded traces. These sources of possible error could be eliminated or minimized by, (1) use of more sensitive strain gages with larger output per unit strain, and, (2) recording velocity waveform in addition to simultaneous acceleration and drive spindle strain. This would require the use of a strain gage type vibration pickup; the Consolidated instrument used in the tests described was a self-exciting, piezo-electric type whose output could not be matched to the recorder galvanometer.

Other configurations of bearing support, in particular that with the light spring mounted in the horizontal plane, were observed. Bearing motion was pronounced and the spring appeared to be operating without bottoming. This constituted a system with non-symmetrical bearing stiffness. Although not within the scope of this study, this configuration is of considerable interest any may form a logical extension to this work.

4. THEORETICAL ANALYSIS

A model representative of the rotating system is shown in Fig. 20. Component names and general nomenclature associated with the physical system were retained wherever possible.

Values of the physical properties of the system used in this analysis differ somewhat from those listed in Table I. Only three masses are defined in the theoretical model; the mass of the rotor, m_2, and the masses of the left and right-hand bearing complexes, m_1 and m_3, respectively.

4.1 Equivalent Mass Lumping

Any physical system can be said to have infinite degrees of freedom in that it is composed of an infinite number of point masses. In some cases less significant masses are ignored completely. An example is the elementary spring-mass system. The center of gravity of the spring is obviously displaced during oscillations and it therefore constitutes a mass in motion. Since the principal mass of the system is very often several orders of magnitude greater than that of the spring and the displacement of the spring mass is so small its contribution to the system is insignificant. For the system under consideration here, an attempt is made to formulate a logical expression to reflect the contribution of the motion of the shaft to the total energy of the system. The kinetic energy of the actual shaft in vibration will be referred to as the shaft energy. The shaft energy will vary for each mode of vibration. Figure 21 shows, in a representative manner, the three modes of vibration for the three mass system. It is easily seen that no single factor will suffice in apportioning the mass of the shaft among the masses in the model. The first mode shown requires that the contribution be made solely to the rotor. The other modes indicate that the bearing masses should be increased by some factor but that the rotor mass need not be modified. If the elastic line of the shaft is assumed to be parabolic, eight-fifteenths of the shaft mass should be added to that of the rotor for similarity. If the other modes were calculated on this basis they would be in error. Ideally an assumption should be

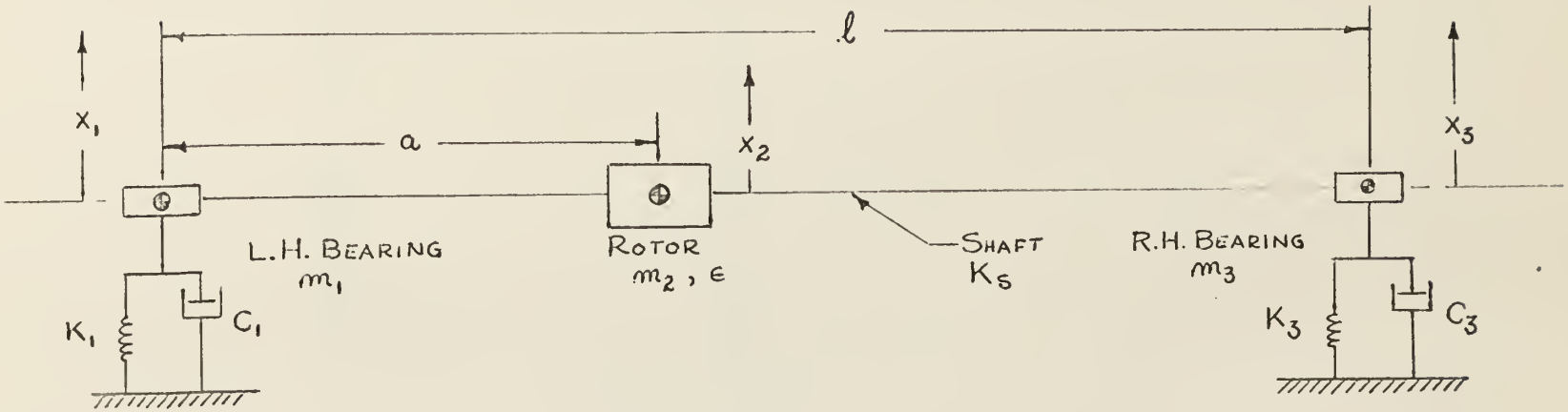

FIGURE 20

REPRESENTATION OF ROTATING SYSTEM

Figure 21

Representative Modes of Vibration

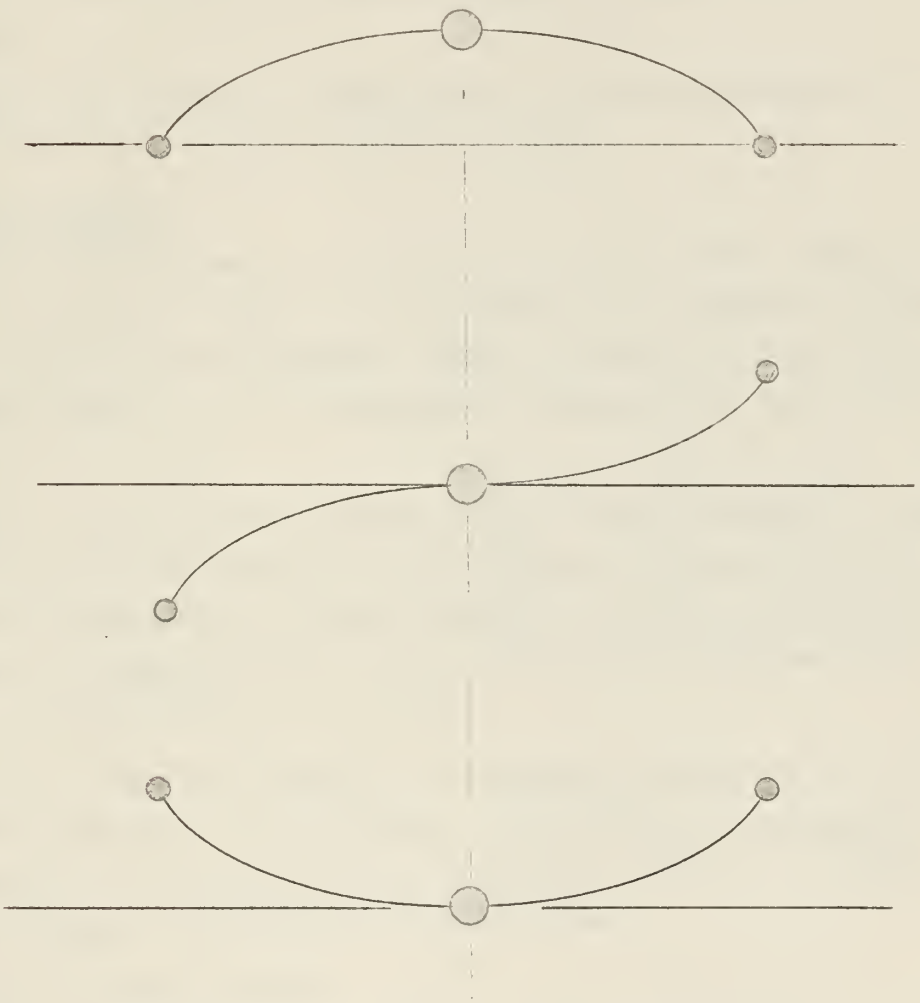

made as to the apportionment for each mode, the mode shapes calculated and the respective factors revised. Due to the relatively small mass associated with the actual shaft an iteration of this kind was not felt to be necessary. A factor of one-third was taken; the mass of each bearing and that of the rotor was increased by one-third the mass of the adjacent shaft section(s). The mass of the overhung drive disk, being so physically close to the left-hand bearing, was lumped with that bearing complex.

Table VII, Equivalent Lumped Masses, lists the calculated values of the three masses in the theoretical model.

4.2 Mass Dynamics

Free body diagrams of the three masses with forces acting during rotation are shown in Fig. 22. The differential equations of motion based on the free body diagrams reduce to a system of six simultaneous algebraic equations. The development is shown on the pages following Fig. 22.

Had a solution in the form $X_i = R_i e^{\delta t}$ been assumed, the system could have been described in three equations with complex coefficients. Computer programming of complex expressions requires a somewhat more demanding technique, and, for this reason, the expressions with real quantities throughout were selected.

The six equations describe the theoretical model of the rotating system in damped, forced vibration. As shown in the last page of the development, the system of general equations reduce to a specific case for the rotor at the middle of the shaft span.

4.2.1 Program CRTSPD

The six simultaneous algebraic equations are the basis of the computer program CRTSPD (Critical Speed). Fortran, [11], coding was used. A program flow chart indicates the logic and progress of the computations in the computer. A sample program is included in Appendix B.

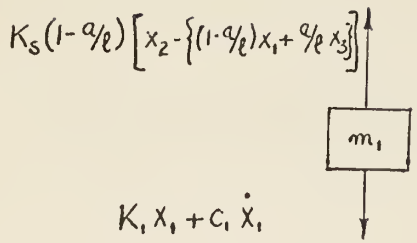

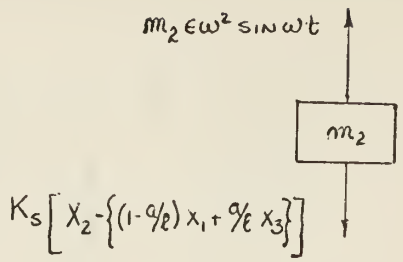

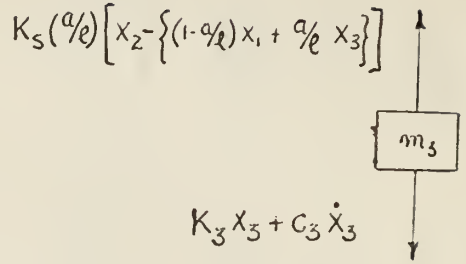

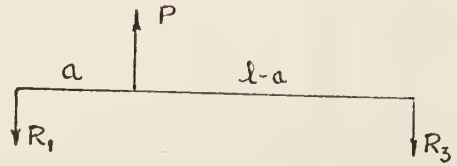

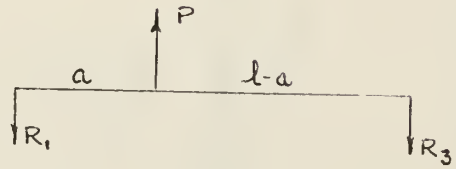

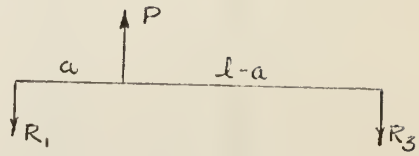

MOMENTS ABOUT ③

$P \times (\ell - a) - R_1 \times \ell = 0$

$R_1 = \left(\frac{\ell - a}{\ell}\right) P = (1 - a/\ell)\, P$

Σ VERTICAL FORCES

$P = R_1 + R_3$

MOMENTS ABOUT ①

$P \times a - R_3 \times \ell = 0$

$R_3 = a/\ell \times P$

FIGURE 22

FREE BODY DIAGRAMS

Rotor mass:

$$m_R = \frac{14.48}{386} + \frac{2}{3} \quad (.0544/386)\ (20.25) = 0.394$$

Left-hand bearing complex mass:

$$m_1 = \frac{7.88}{386} + \frac{1}{3} \quad (.0544/386)\ (20.25) + 2.035 = 0.0270$$

Right-hand bearing complex mass:

$$m_3 = 7.88 + 1\ (.0544/386)\ (20.25) = 0.0220$$

Table VII

EQUIVALENT LUMPED MASSES

Significant Mass	W(lbs.)	M(m.u.)	
L.H. Bearing complex	10.434	0.0270	m_1
Rotor	15.213	0.0394	m_2
R.H. Bearing complex	8.501	0.0220	m_3

Mass Ratios:

$$m_1/m_2 = 0.0270/0.394 = 0.6858 = \mu_1$$

$$m_3/m_2 = 0.0220/0.394 = 0.5588 = \mu_3$$

EQUATIONS OF MOTION

$m_1 = W_1/g$, LB-SEC^2/IN. ; $m_2 = W_R/g$, LB-SEC^2/IN. ; $m_3 = W_3/g$, LB-SEC^2/IN. ; $g = 386$ IN./SEC^2

K_1 = L.H. SUPPORT SPRING STIFFNESS, LB./IN. ; K_S = SHAFT SPRING STIFFNESS, LB/IN.

K_3 = R.H. SUPPORT SPRING STIFFNESS, LB./IN. ; $\mu_1 = m_1/m_2$; $\mu_3 = m_3/m_2$

C_1 = L.H. SUPPORT DAMPING CONSTANT, LB./(IN./SEC) ; C_3 = R.H. SUPPORT DAMPING CONSTANT

$\lambda_1 = C_1/m_2$, SEC^{-1} ; $\lambda_3 = C_3/m_2$, SEC^{-1} ; $\omega_R^2 = K_S/m_2$, SEC^{-2} ; $\omega_1^2 = K_1/m_2$, SEC^{-2} ; $\omega_3^2 = K_3/m_2$, SEC^{-2}

$X_1 = A\sin\omega t + B\cos\omega t$ $\quad$ $X_2 = C\sin\omega t + D\cos\omega t$ $\quad$ $X_3 = E\sin\omega t + F\cos\omega t$

$\dot{X}_1 = \omega A\cos\omega t - \omega B\sin\omega t$ $\quad$ $\dot{X}_2 = \omega C\cos\omega t - \omega D\sin\omega t$ $\quad$ $\dot{X}_3 = \omega E\cos\omega t - \omega F\sin\omega t$

$\ddot{X}_1 = -\omega^2 A\sin\omega t - \omega^2 B\cos\omega t$ $\quad$ $\ddot{X}_2 = -\omega^2 C\sin\omega t - \omega^2 D\cos\omega t$ $\quad$ $\ddot{X}_3 = -\omega^2 E\sin\omega t - \omega^2 F\cos\omega t$

L.H. BEARING, m_1

$$m_1\ddot{x}_1 = -K_1 x_1 - C_1\dot{x}_1 + K_S\left[(1-a/\ell)\{x_2 - ([1-a/\ell]x_1 + [a/\ell]x_3)\}\right]$$

$$\mu_1(-\omega^2 A\sin\omega t - \omega^2 B\cos\omega t) = (A\sin\omega t + B\cos\omega t)\left[-\omega_1^2 - \omega_R^2(1-a/\ell)^2\right] - \lambda_1(\omega A\cos\omega t - \omega B\sin\omega t)$$
$$+ (C\sin\omega t + D\cos\omega t)(\omega_R^2)(1-a/\ell) + (E\sin\omega t + F\cos\omega t)(-\omega_R^2)(a/\ell)(1-a/\ell)$$

$$\sin\omega t\left\{A\left[\mu_1\omega^2 - \omega_1^2 - \omega_R^2(1-a/\ell)^2\right] + B[\lambda_1\omega] + C[\omega_R^2(1-a/\ell)] + 0 + E[-\omega_R^2(a/\ell)(1-a/\ell)] + 0\right\} = 0$$

$$\cos\omega t\left\{A[-\lambda_1\omega] + B\left[\mu_1\omega^2 - \omega_1^2 - \omega_R^2(1-a/\ell)^2\right] + 0 + D[\omega_R^2(1-a/\ell)] + 0 + F[-\omega_R^2(a/\ell)(1-a/\ell)]\right\} = 0$$

ROTOR, m_2

$$m_2 \ddot{x}_2 = -K_s\left[x_2 - \{(1-a/\ell)x_1 + (a/\ell)x_3\}\right] + m_2 \epsilon \omega^2 \sin\omega t$$

$$-\omega^2 C\sin\omega t - \omega^2 D\cos\omega t = (A\sin\omega t + B\cos\omega t)(1-a/\ell)\omega_R^2 - (C\sin\omega t + D\cos\omega t)\omega_R^2 \cdot$$
$$-(E\sin\omega t + F\cos\omega t)(a/\ell)(\omega_R^2) + \epsilon\omega^2 \sin\omega t$$

$$\sin\omega t\left\{A\left[\omega_R^2(1-a/\ell)\right] + 0 + C\left[\omega^2 - \omega_R^2\right] + 0 + E\left[-\omega_R^2(a/\ell)\right] + 0 + \epsilon\omega^2\right\} = 0$$

$$\cos\omega t\left\{0 + B\left[\omega_R^2(1-a/\ell)\right] + 0 + D\left[\omega^2 - \omega_R^2\right] + 0 + F\left[-\omega_R^2(a/\ell)\right]\right\} = 0$$

R.H. BEARING, m_3

$$m_3 \ddot{x}_3 = -K_3 x_3 - C_3 \dot{x}_3 + K_s\left[(a/\ell)\left(x_2 - \{(1-a/\ell)x_1 + (a/\ell)x_3\}\right)\right]$$

$$\mu_3(-\omega^2 E\sin\omega t - \omega^2 F\cos\omega t) = (A\sin\omega t + B\cos\omega t)(-\omega_R^2)(a/\ell)(1-a/\ell) + (C\sin\omega t + D\cos\omega t)\omega_R^2(a/\ell)$$
$$+(E\sin\omega t + F\cos\omega t)(-\omega_3^2 - \omega_R^2[a/\ell]^2) - \lambda_3(\omega E\cos\omega t - \omega F\sin\omega t)$$

$$\sin\omega t\left\{A\left[-(1-a/\ell)(a/\ell)\omega_R^2\right] + 0 + C\left[(a/\ell)\omega_R^2\right] + 0 + E\left[\mu_3\omega^2 - \omega_3^2 - (a/\ell)^2\omega_R^2\right] + F\left[\lambda_3\omega\right]\right\} = 0$$

$$\cos\omega t\left\{0 + B\left[-(a/\ell)(1-a/\ell)\omega_R^2\right] + 0 + D\left[(a/\ell)\omega_R^2\right] + E\left[-\lambda_3\omega\right] + F\left[\mu_3\omega^2 - \omega_3^2 - (a/\ell)^2\omega_R^2\right]\right\} = 0$$

MATRIX OF COEFFICIENTS

A	B	C	D	E	F	K
$(1-a/\ell)\,\omega_R^2$	0	$\omega^2-\omega_R^2$	0	$(a/\ell)\omega_R^2$	0	$-\epsilon\omega^2$
0	$(1-a/\ell)\,\omega_R^2$	0	$\omega^2-\omega_R^2$	0	$(a/\ell)\omega_R^2$	0
$-(1-a/\ell)(a/\ell)\,\omega_R^2$	0	$(a/\ell)\omega_R^2$	0	$\mu_3\omega^2-\omega_3^2-(a/\ell)^2\omega_R^2$	$\lambda_3\omega$	0
$-\lambda_1\omega$	$\mu_1\omega^2-\omega_1^2-(1-a/\ell)^2\omega_R^2$	0	$(1-a/\ell)\omega_R^2$	0	$-(a/\ell)(1-a/\ell)\omega_R^2$	0
$\mu_1\omega^2-\omega_1^2-(1-a/\ell)^2\omega_R^2$	$\lambda_1\omega$	$(1-a/\ell)\omega_R^2$	0	$-(a/\ell)(1-a/\ell)\omega_R^2$	0	0
0	$-(a/\ell)(1-a/\ell)\omega_R^2$	0	$(a/\ell)\omega_R^2$	$-\lambda_3\omega$	$\mu_3\omega^2-\omega_3^2-(a/\ell)^2\omega_R^2$	0

MATRIX OF COEFFICIENTS - ROTOR MIDSPAN ($a = \ell/2$)

A	B	C	D	E	F	K
$\omega_R^2/2$	0	$\omega^2 - \omega_R^2$	0	$\omega_R^2/2$	0	$-\epsilon\omega^2$
0	$\omega_R^2/2$	0	$\omega^2 - \omega_R^2$	0	$\omega_R^2/2$	0
$-\omega_R^2/4$	0	$\omega_R^2/2$	0	$\mu_3\omega^2 - \omega_3^2 - \omega_R^2/4$	$\lambda_3\omega$	0
$-\lambda_1\omega$	$\mu_1\omega^2 - \omega_1^2 - \omega_R^2/4$	0	$\omega_R^2/2$	0	$-\omega_R^2/4$	0
$\mu_1\omega^2 - \omega_1^2 - \omega_R^2/4$	$\lambda_1\omega$	$\omega_R^2/2$	0	$-\omega_R^2/4$	0	0
0	$-\omega_R^2/4$	0	$\omega_R^2/2$	$-\lambda_3\omega$	$\mu_3\omega^2 - \omega_3^2 - \omega_R^2/4$	0

Figure 23

Flow Chart PROGRAM CRTSPD

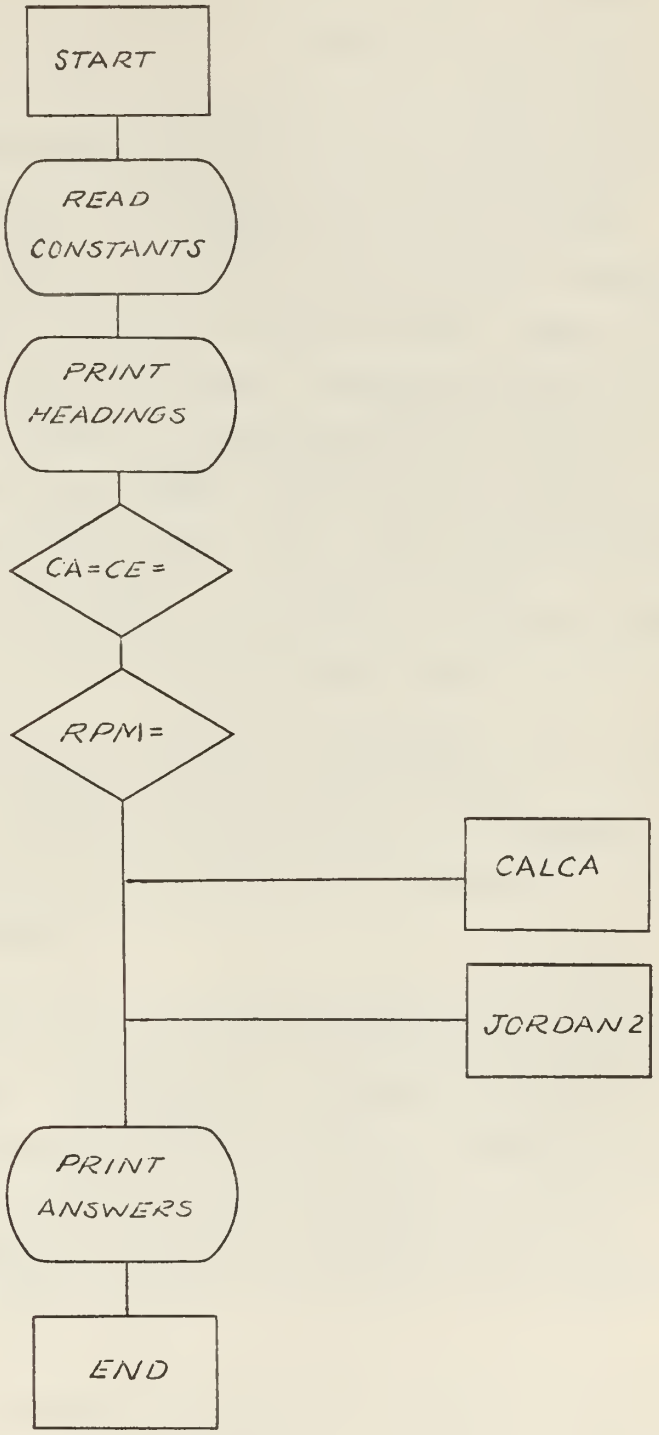

The dimension statement apportions storage space for the arrays representing the augmented matrix of coefficients of the algebraic equations of motion and the values of their solution, X(6). Column headings for the printout are specified. The constants of the physical system, C1-C6, represent ω_R^2, ω_1^2, ω_3^2, μ_1, μ_3, and ϵ, respectively. CA is the coded form of the damping constant at the left-hand bearing. CE is the corresponding damping constant for the right-hand bearing. These constants were set equal to one another for all calculations. The value so assigned is hereafter referred to as the symmetrical damping constant. The DO 10 statement defines the range of RPM. Omega is then defined in terms of RPM. Subroutine CALCA, to which all factors necessary for the calculation of the elements of the augmented matrix have been made available through use of the COMMON statement, then calculates each element according to the specified value of RPM. The resulting numerical array, A, common to Subroutine JORDAN2, is solved as a set of simultaneous equations. The values of the solution are returned to the main program and amplitudes of mass motion and associated phase angles are calculated.

Calculated system response was initially investigated over a broad range of speeds. Results indicated that the critical speeds of the system lay between 200 and 900 RPM. Calculations for unit steps of RPM were selected so that variations of response with speed would be well defined in the critical regions.

Values initially chosen for the damping constant were somewhat arbitrary. Calculations for very small and very large values of the damping constant were made. Investigation of system response for all possible combinations of damping constants at the two bearings was obviously impractical. The case in which the two constants would be kept equal seemed to be a suitable starting point. Hereafter the term "symmetrical damping constant" or merely "c" will be used to describe the stated relationship.

From the preliminary computer calculations it was noted that the most profitable region for close investigation was defined by small values of c, i.e., between 0.0 and 3.0 lbs/(in./sec.).

Computer runs were made for no damping, (bearings supported by the springs alone), and for damping values up to 3.0 lbs./(in./sec.) in steps of 0.5 lbs./(in./sec.). The case, supposedly analogous to the experimental test for damping of 1.77 lbs.(in./sec.), was also run on the computer. A value of exceptionally large damping, 10,000 lbs./(in./sec.), was assigned to produce calculated response corresponding to the fixed-bearing experimental test. Results of the computer calculations described are shown graphically in Figs. 24-41. The three modes of vibration associated with no damping are shown in Fig. 24.

4.2.2 Critical and Optimum Damping

Ordinarily the concept of critical damping is reserved for systems with few degrees of freedom in free vibration. In the simple, single degree of freedom, spring-mass-dashpot system as treated for example by Burton, {12}, the differential equation of motion is developed as follows:

$$m\ddot{x} = -c\dot{x} - kx \qquad \text{ASSUMING } x = Re^{\delta t} \qquad \delta^2 + \frac{c}{m}\delta + \frac{k}{m} = 0$$

$$\delta = \frac{-c \pm \sqrt{c^2 - 4mk}}{2m}$$

FOR $c=0$,

$$\delta = \pm i\sqrt{k/m}$$

$$x = Re^{\pm i\sqrt{k/m}\,t}$$

FOR CRITICAL DAMPING,

$$c^2 = 4mk \qquad c = 2\sqrt{mk}$$

$$\delta = -\frac{c}{2m}$$

$$x = Re^{-\frac{c}{2m}t}$$

The finite value of c for which the term in the radical reduces to zero is referred to as the critical damping constant. From the resulting expression for the response of the system at critical damping it can be seen that the system does not oscillate; any initial displacement from equilibrium is followed by a direct return of the mass to the equilibrium position. Larger values of damping result in a similar response but the time to return to the equilibrium position is increased. For infinite damping the time for return is infinite, or, in other words, the mass never returns to its initial position. The pertinent part of the definition of critical damping is that it specifies the minimum value of damping for which the mass does not oscillate in response to a disturbance. For physical systems damping is always greater than or equal to zero.

The single degree of freedom system is described by a quadratic in δ. If this treatment is extended to a system with two degrees of freedom with both masses subject to damping a quartic expression in δ results. In this case two damping constants govern the nature of the imaginary parts of the two pairs of complex roots. Generally then, for a system of n masses there will be an expression of degree 2n in δ and n damping constants will govern the nature of the n conjugate pairs of complex roots.

Applying this treatment to the system under investigation results in a sixth degree expression in δ.

$$\xi = \mu_1\mu_3 \qquad \mu_T = \mu_1 + \mu_3 \qquad \lambda_1 = \lambda_3 = \lambda \qquad V = \omega_1^2 + \omega_k^2/4 \qquad \omega_1^2 = \omega_3^2 \qquad Z = \omega_k^2$$

$$\xi\delta^6 + \mu_T\lambda\delta^5 + (V\mu_T + \xi Z + \lambda^2)\delta^4 + (2V + Z\mu_T)\delta^3 + (V^2 + VZ\mu_T + Z\lambda^2 - \frac{Z^2}{4}\mu_T - \frac{Z^2}{16})\delta^2$$

$$+ (2VZ - \frac{Z^2}{2})\delta + V^2Z + \frac{Z^3}{16} - \frac{VZ^2}{2} = 0$$

Certain properties of the roots can be predicted from physical considerations alone. Since only two of the masses are subject to damping there will be only two governing damping constants. One mode of oscillation will be present no matter what values of damping are assigned. For certain values of damping the imaginary parts of two of the three complex pairs of roots will vanish.

An extensive analysis of the sixth degree expression is beyond the scope of this study. The computer was used in a limited analysis. Results indicated that, for the masses and stiffnesses involved in the present tests, the imaginary parts of two of the pairs of roots would vanish for damping constants of about 3.0 and 5.0 lbs./(in./sec.) respectively. For these values the system, in free vibration, would exhibit a response somewhat analogous to a less complex system with critical damping.

Figures 24-41 show the calculated response of the system over a range of small damping constants and for one extremely large value.

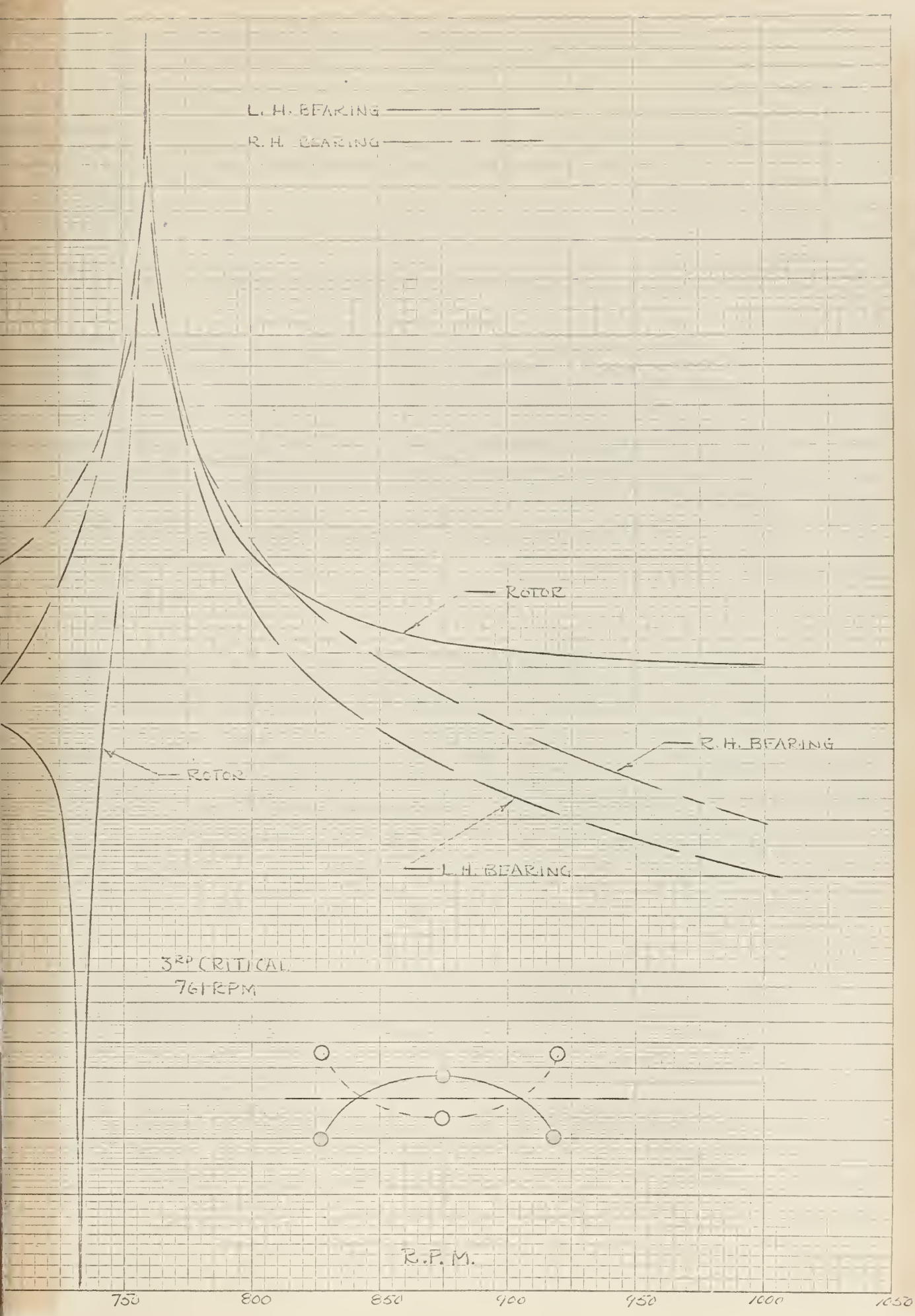
L. H. BEARING
R. H. BEARING
ROTOR
R. H. BEARING
ROTOR
L. H. BEARING
3RD CRITICAL
761 RPM
R.P.M.
750
800
850
900
950
1000
1050

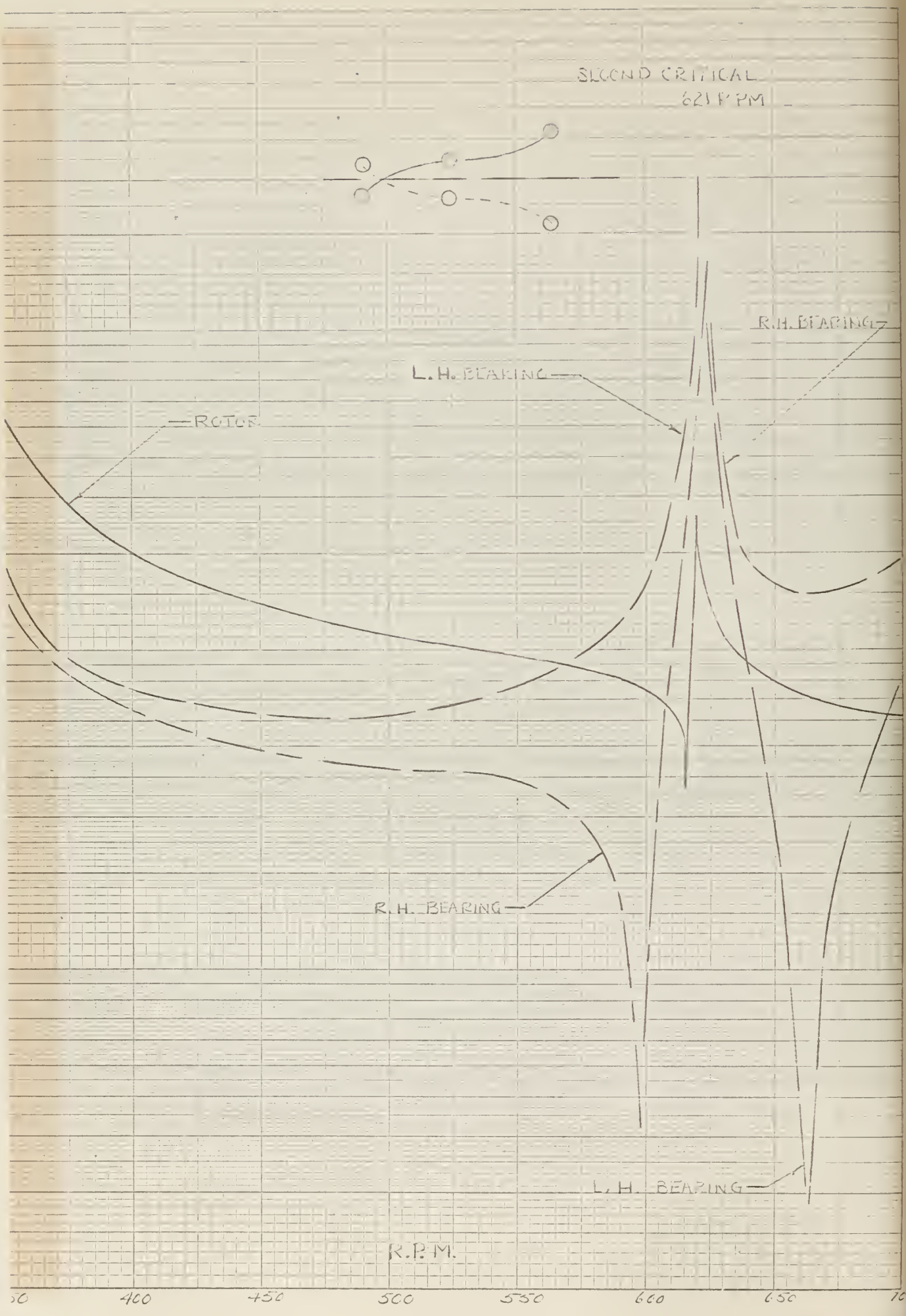
SECOND CRITICAL
621 R.P.M.
R.H. BEARING
L.H. BEARING
ROTOR
R.H. BEARING
L.H. BEARING
R.P.M.
400
450
500
550
600
650

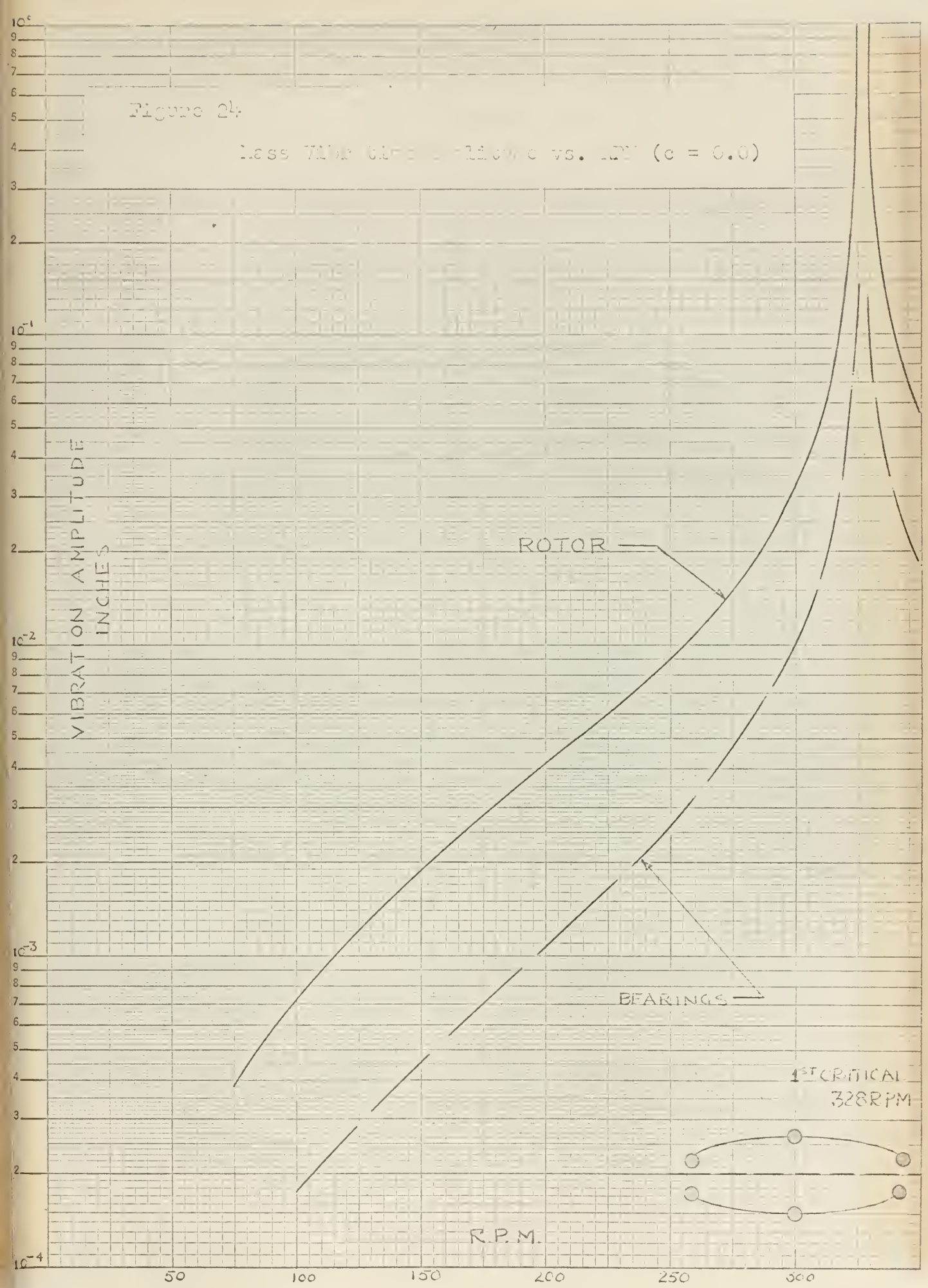
Figure 24
VIBRATION AMPLITUDE INCHES
ROTOR
BEARINGS
1ST CRITICAL 328 RPM
R.P.M.
50
100
150
200
250
300

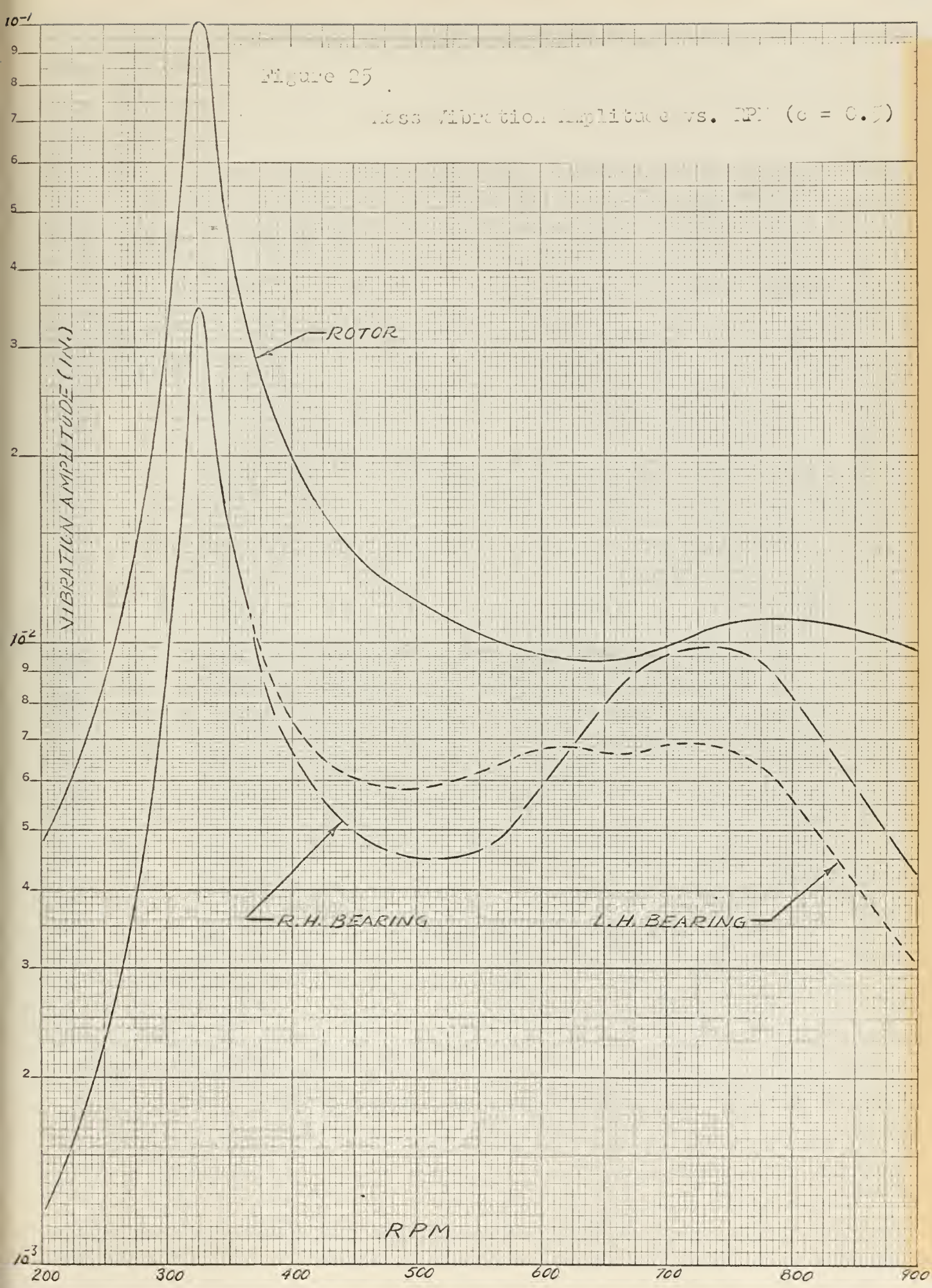
Figure 25
Mass Vibration Amplitude vs. RPM (c = C.)
VIBRATION AMPLITUDE (IN.)
ROTOR
R.H. BEARING
L.H. BEARING
RPM
10⁻¹
10⁻²
10⁻³
200
300
400
500
600
700
800
900

Figure 26

Mass Phase Angle vs. [illegible] (c = 0.5)

Figure 27

Mass Vibration Amplitude vs. RPM (c = 1.0)

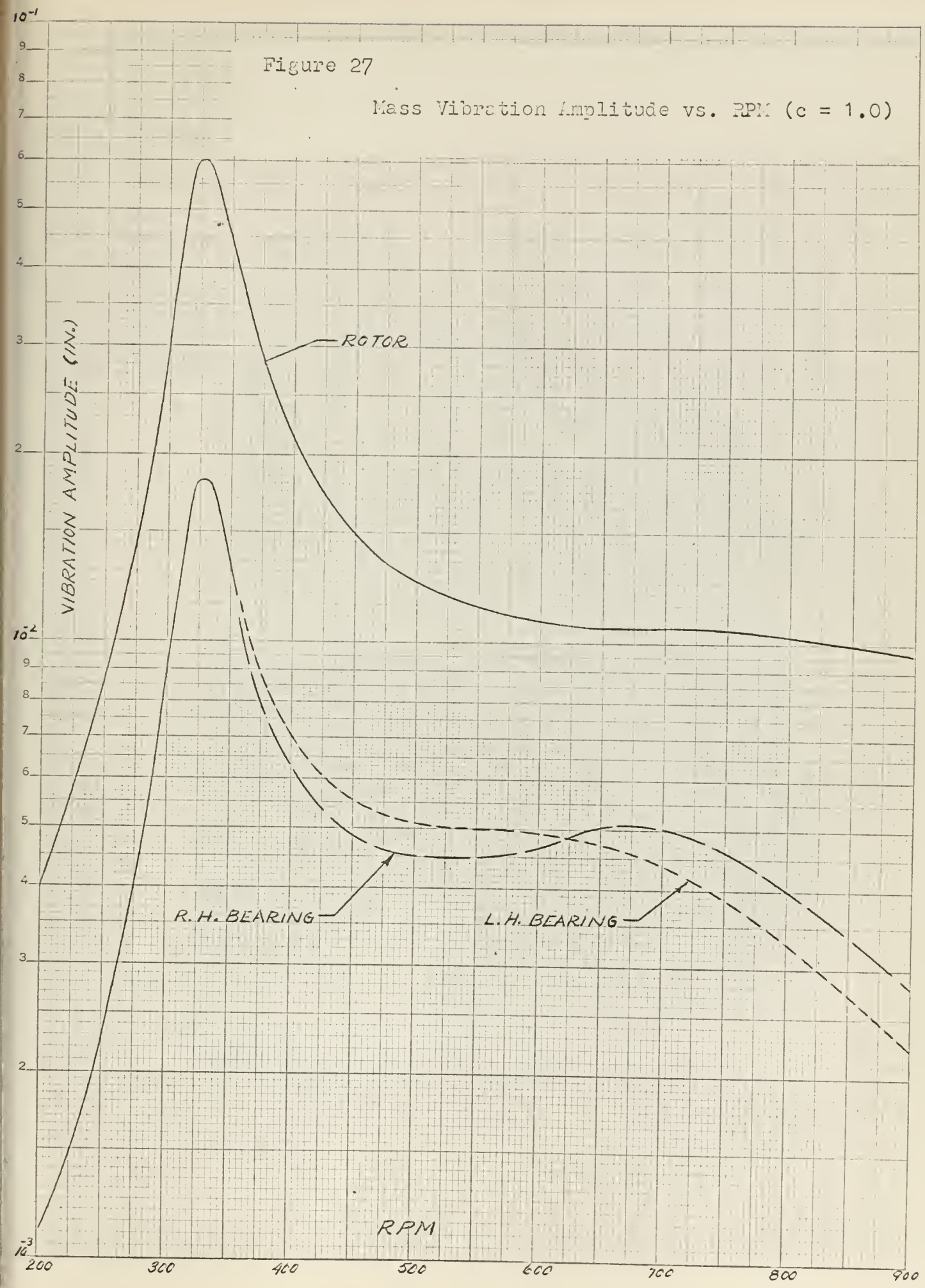

Figure 28

Mass Phase Angle vs. RPM (c = 1.0)

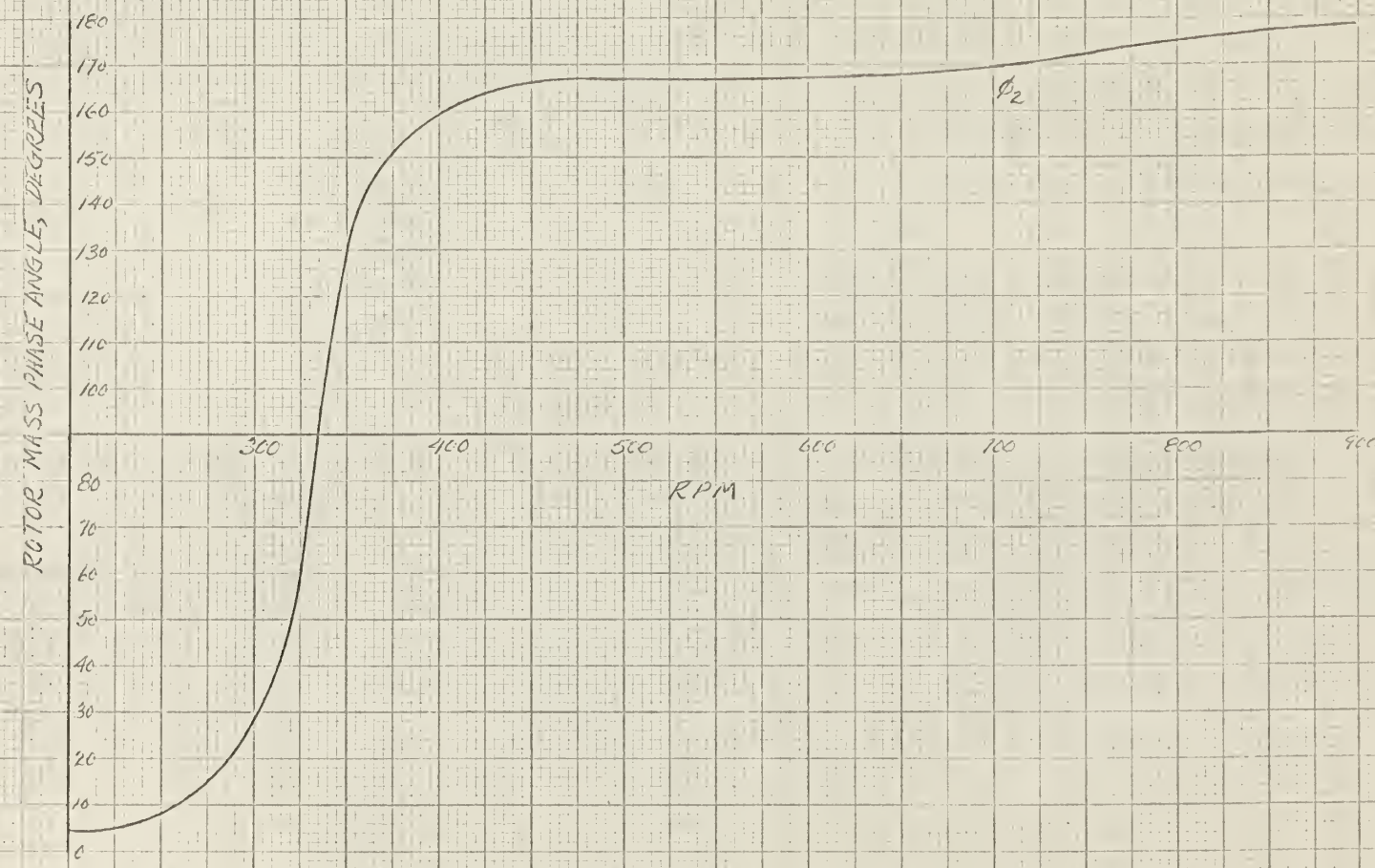

Figure 29 .

Mass Vibration Amplitude vs. RPM (c = 1.5)

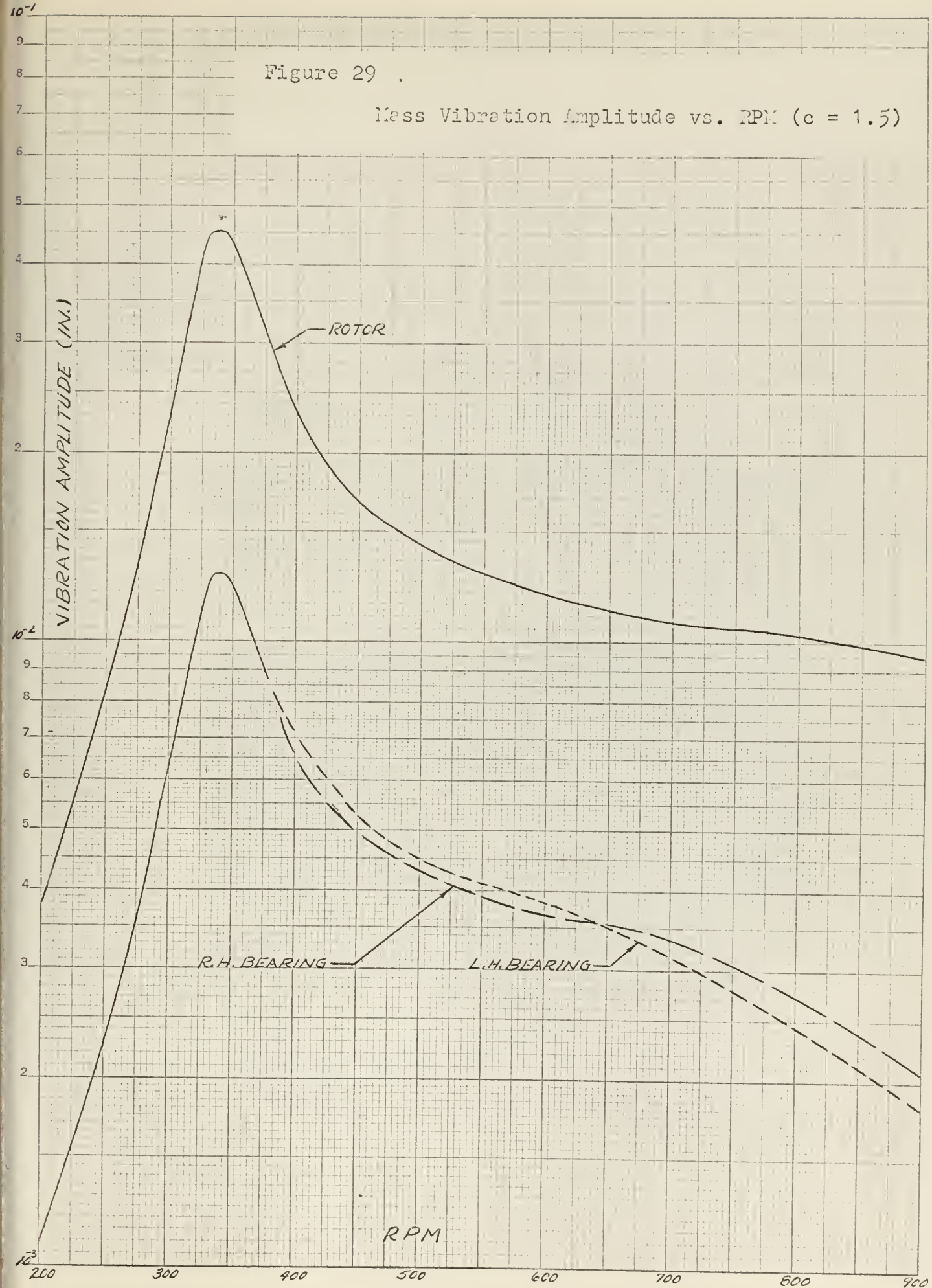

Figure 30

Mass Phase Angle vs. RPM (c = 1.5)

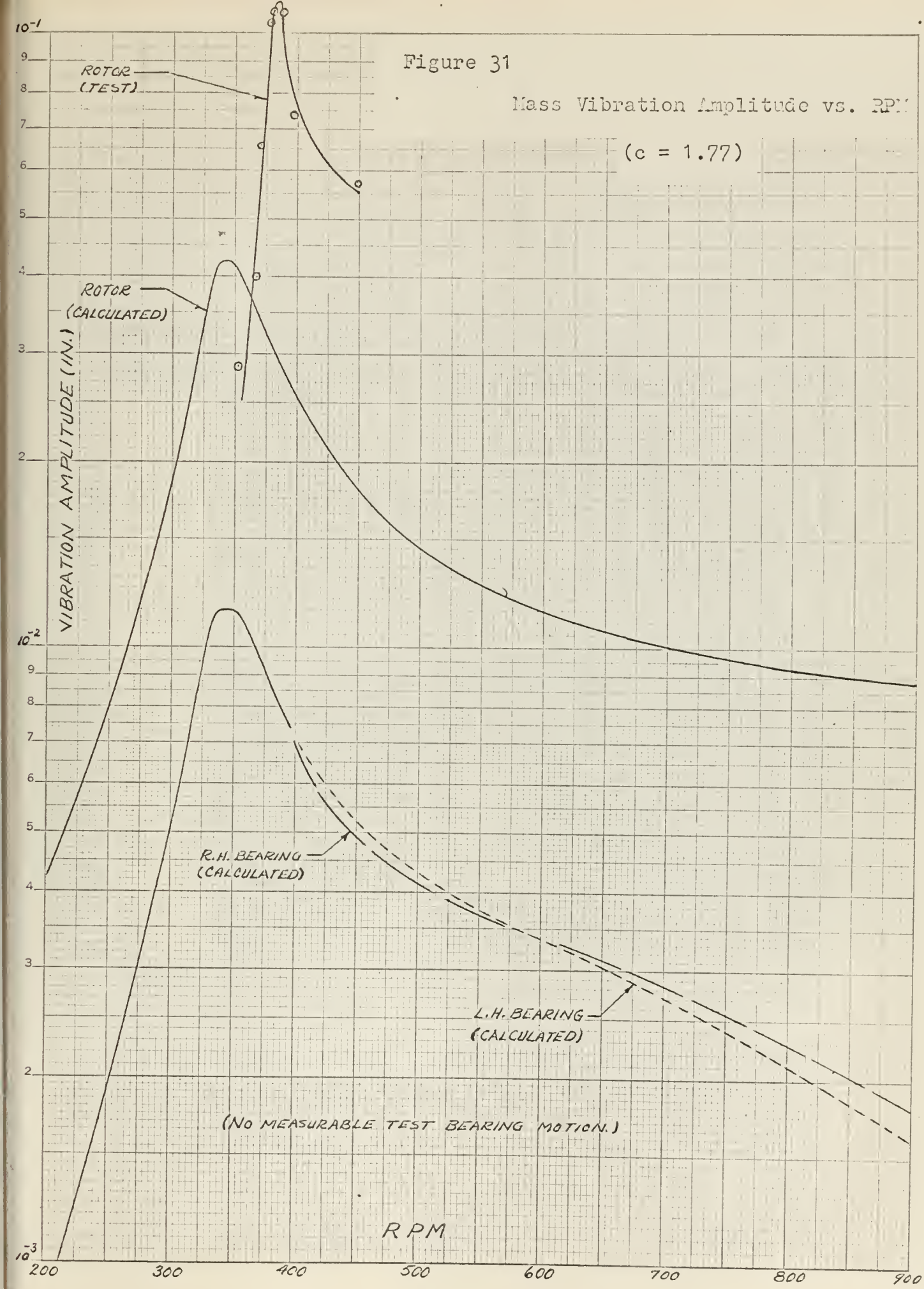
Figure 31
Mass Vibration Amplitude vs. RPM
(c = 1.77)
ROTOR (TEST)
ROTOR (CALCULATED)
VIBRATION AMPLITUDE (IN.)
R.H. BEARING (CALCULATED)
L.H. BEARING (CALCULATED)
(NO MEASURABLE TEST BEARING MOTION.)
RPM
10^{-1}
9
8
7
6
5
4
3
2
10^{-2}
9
8
7
6
5
4
3
2
10^{-3}
200
300
400
500
600
700
800
900

Figure 32

Mass Phase Angle vs. RPM (c = 1.77)

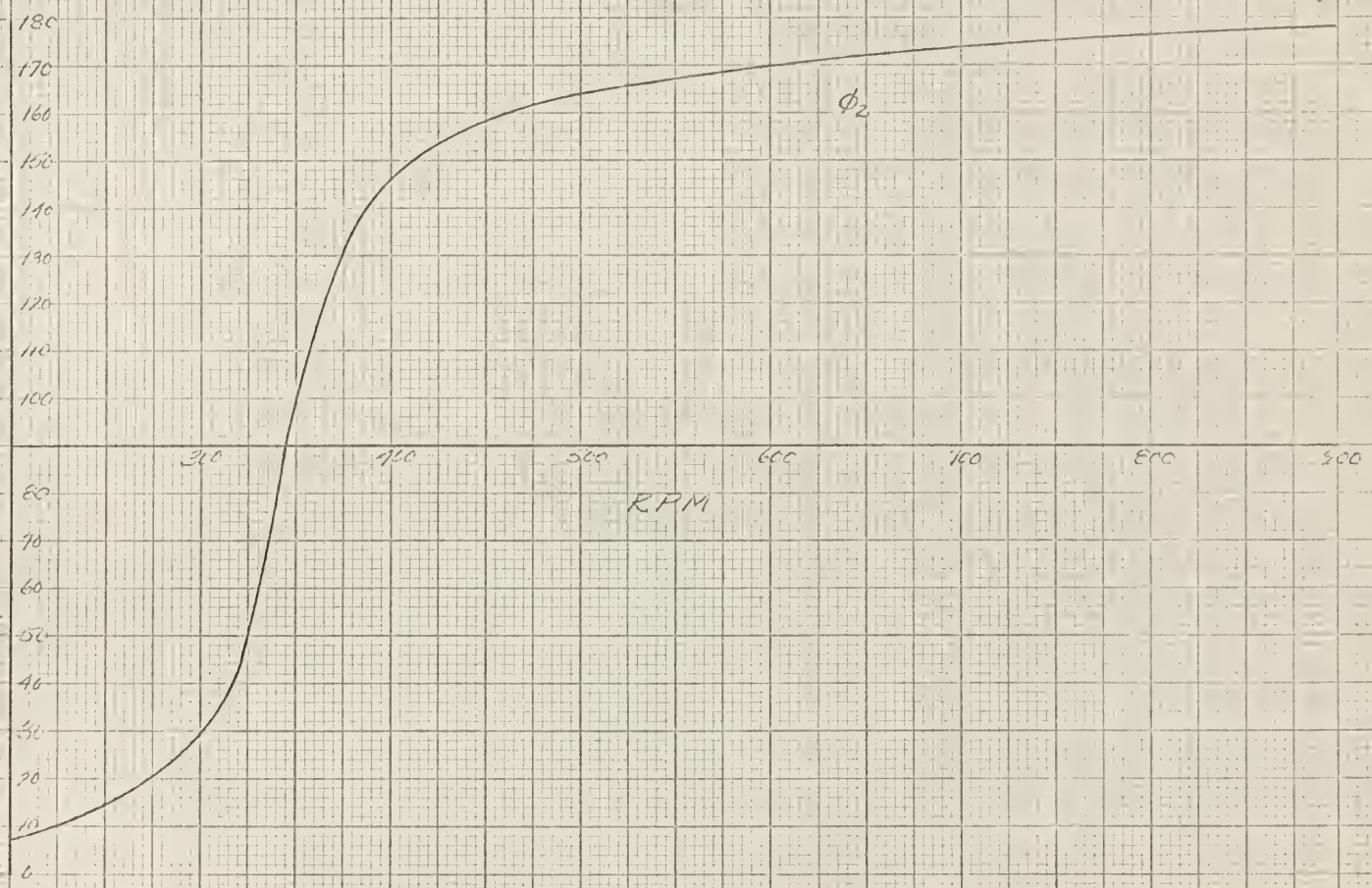

Figure 33

Mass Vibration Amplitude vs. RPM (c = 2.0)

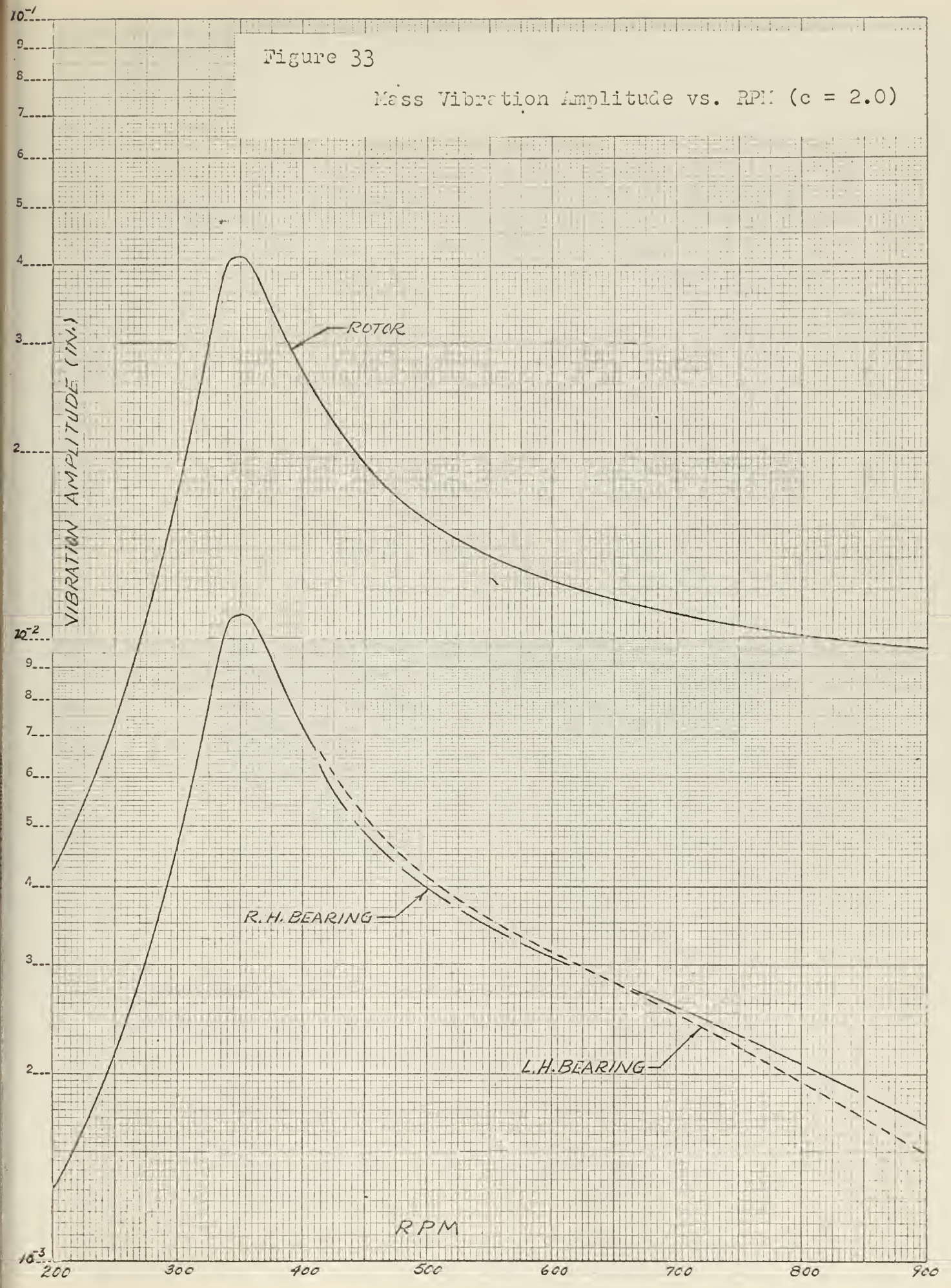

Figure 34

Mass Phase Angle vs. RPM (c = 2.0)

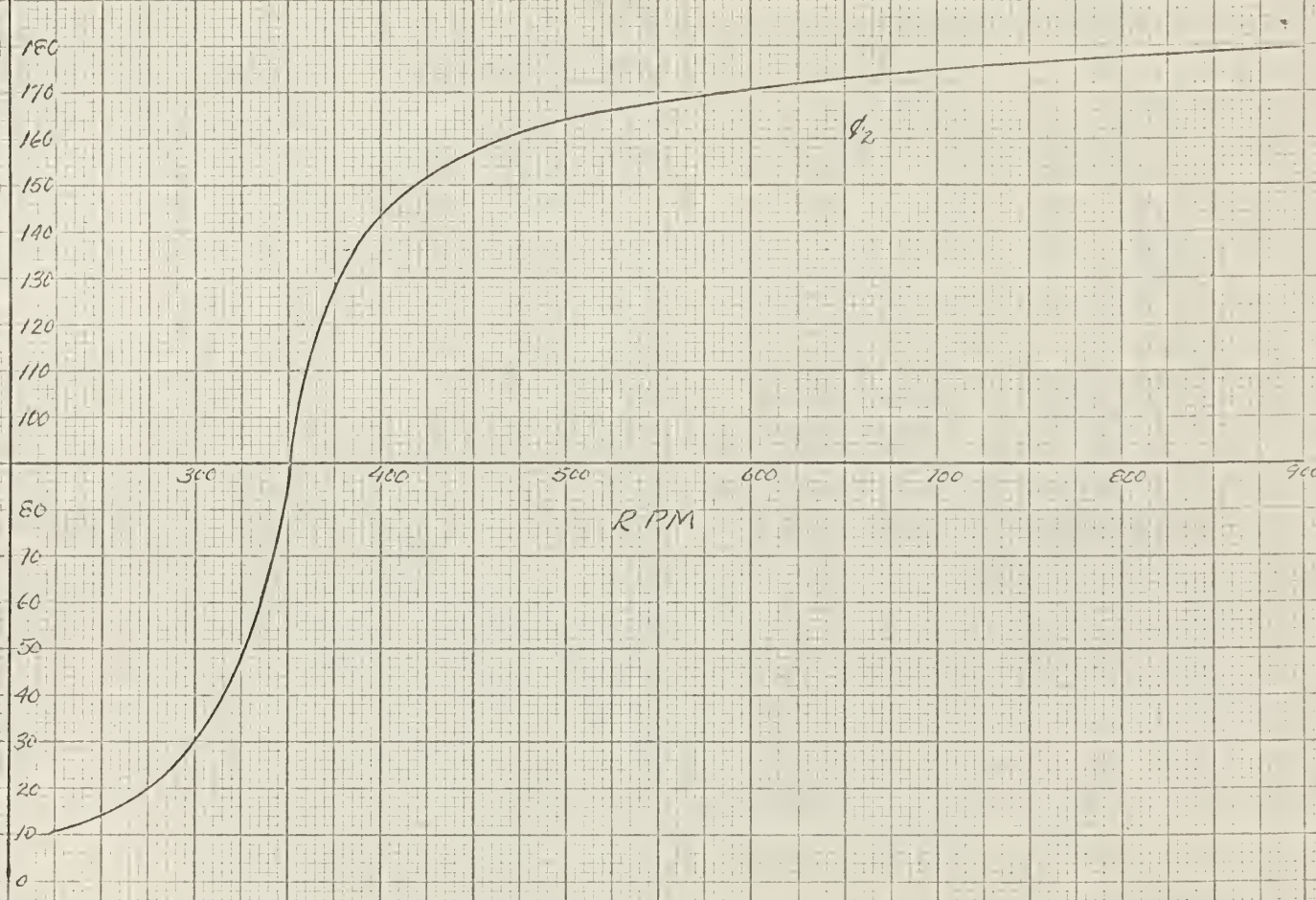

Figure 35

Mass Vibration Amplitude vs. RPM (c = 2.5)

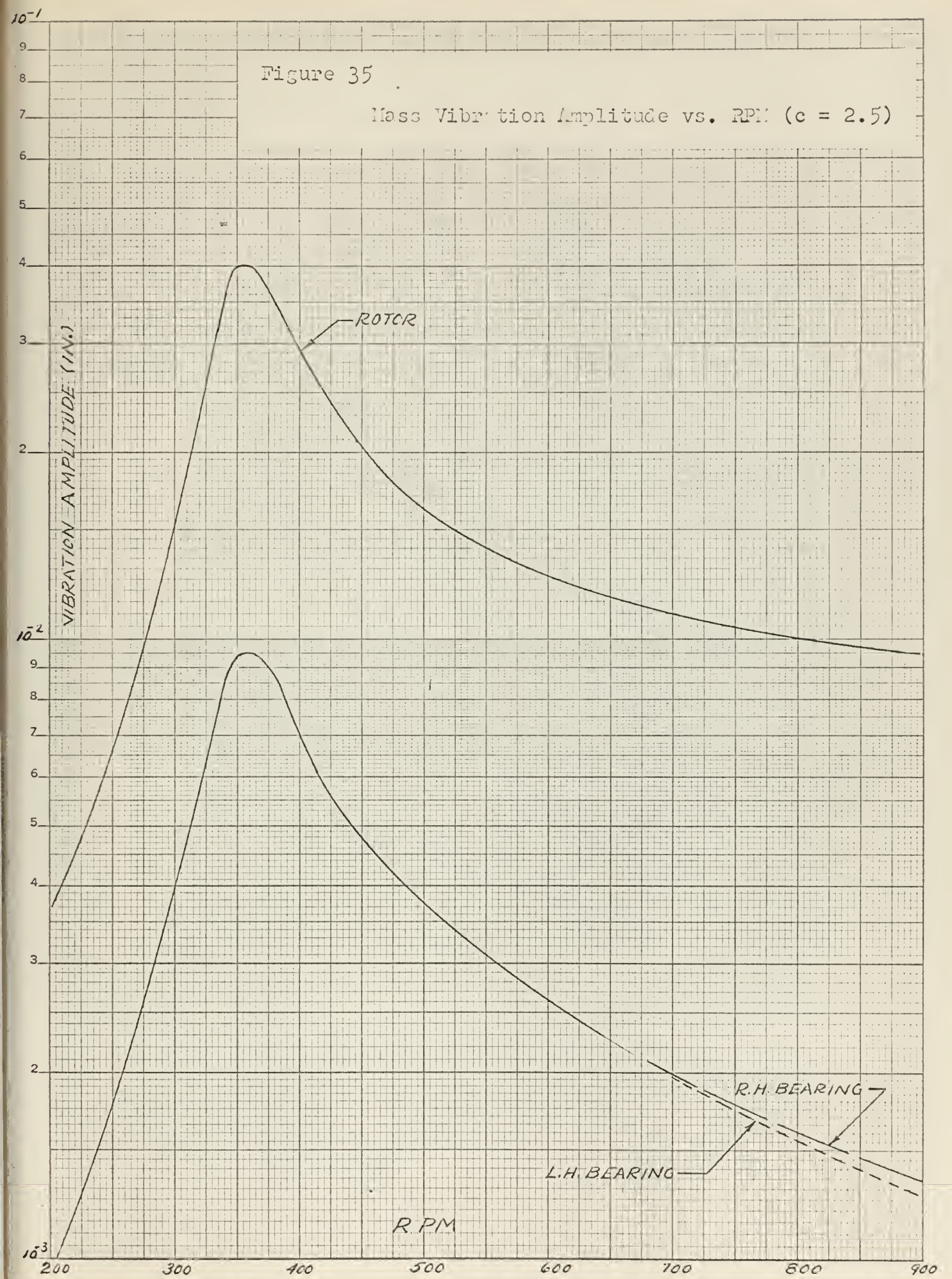

Figure 36

Mass Phase Angle vs. RPM (c = 2.5)

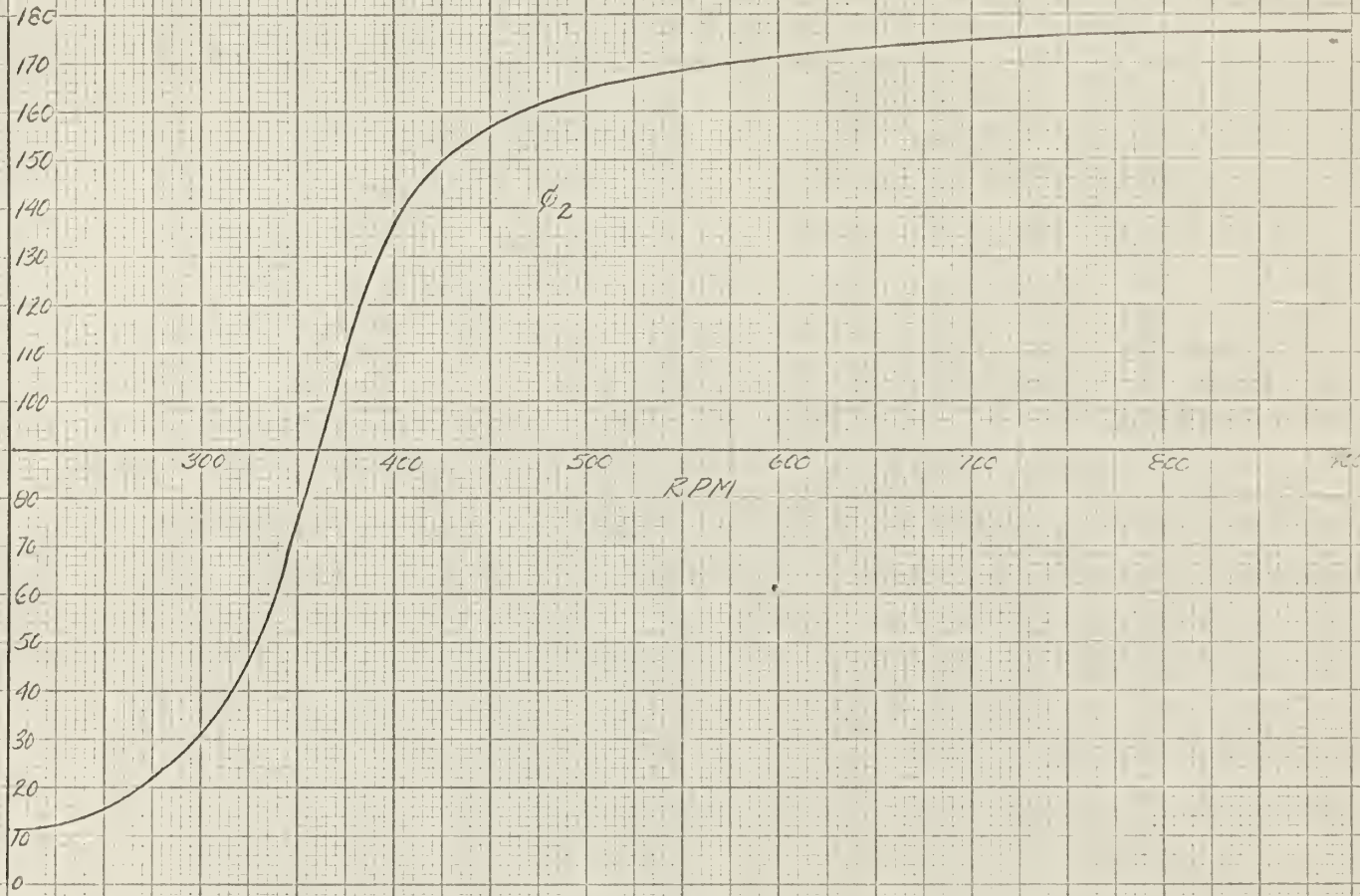

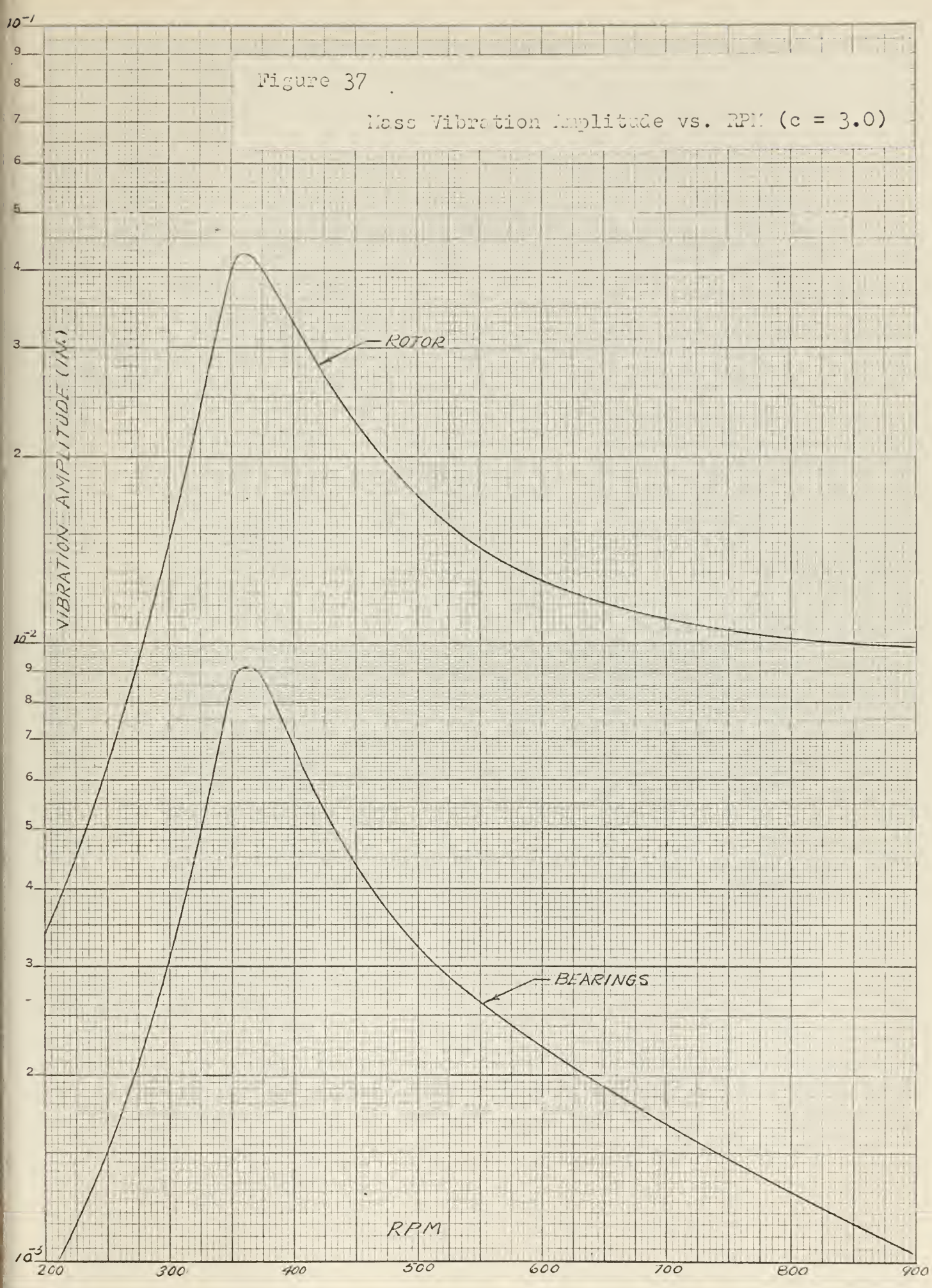
Figure 37
Mass Vibration Amplitude vs. RPM (c = 3.0)
VIBRATION AMPLITUDE (IN.)
ROTOR
BEARINGS
RPM
10⁻¹
9
8
7
6
5
4
3
2
10⁻²
9
8
7
6
5
4
3
2
10⁻³
200
300
400
500
600
700
800
900

Figure 38

Mass Phase Angle vs. RPM (c = 3.0)

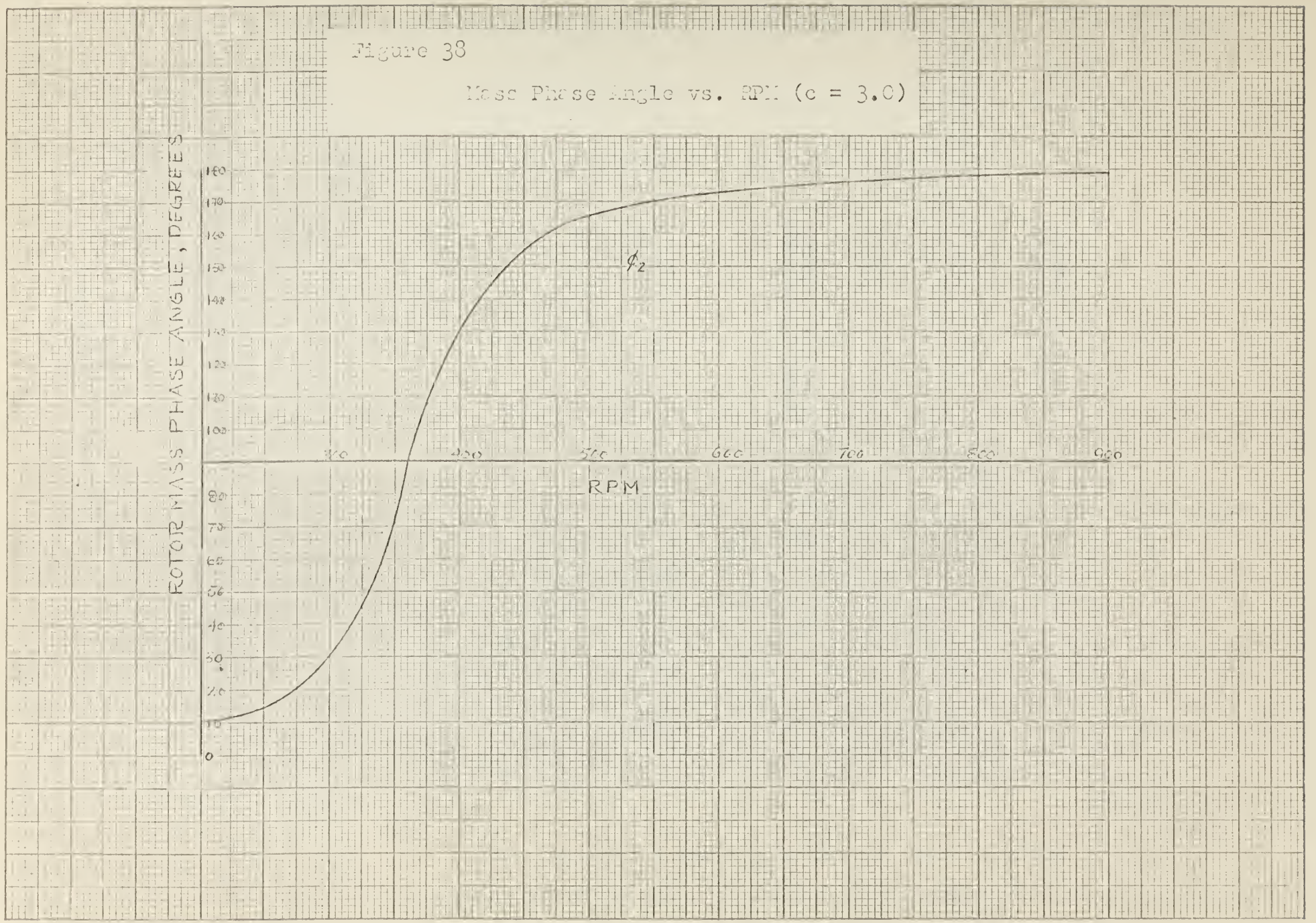

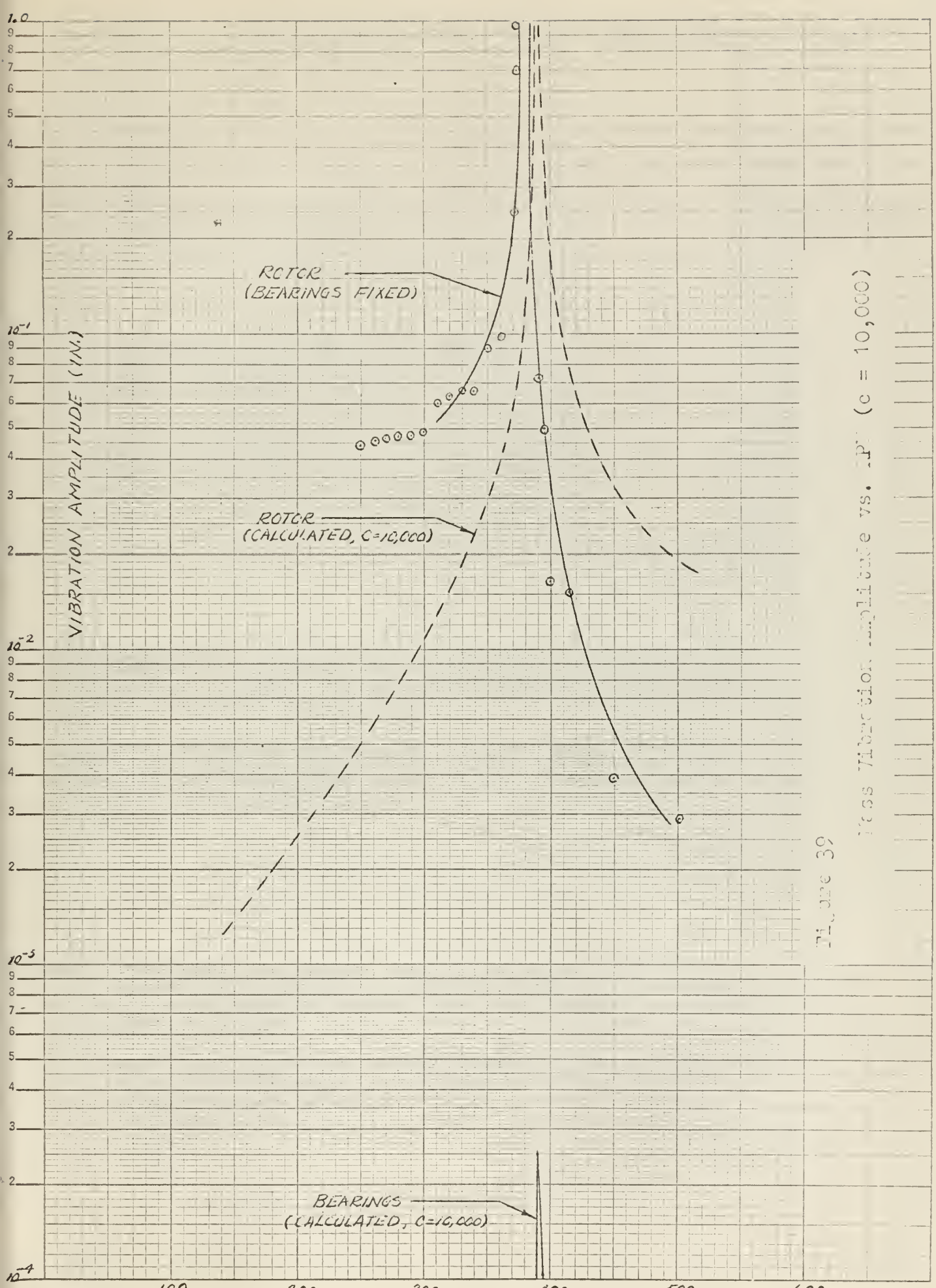

Figure 39

Mass Vibration Amplitude vs. RPM (c = 10,000)

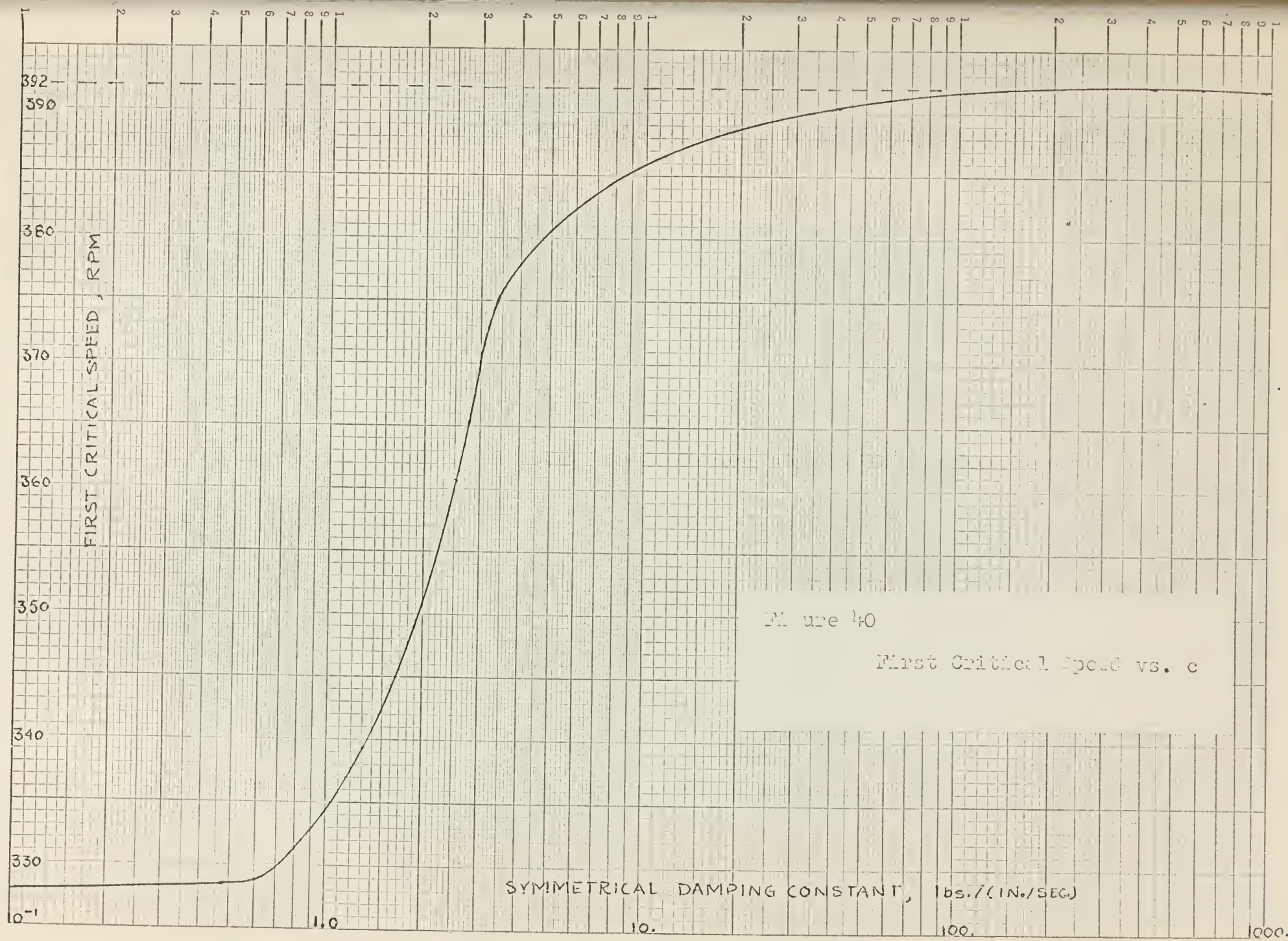

Figure 40

First Critical Speed vs. c

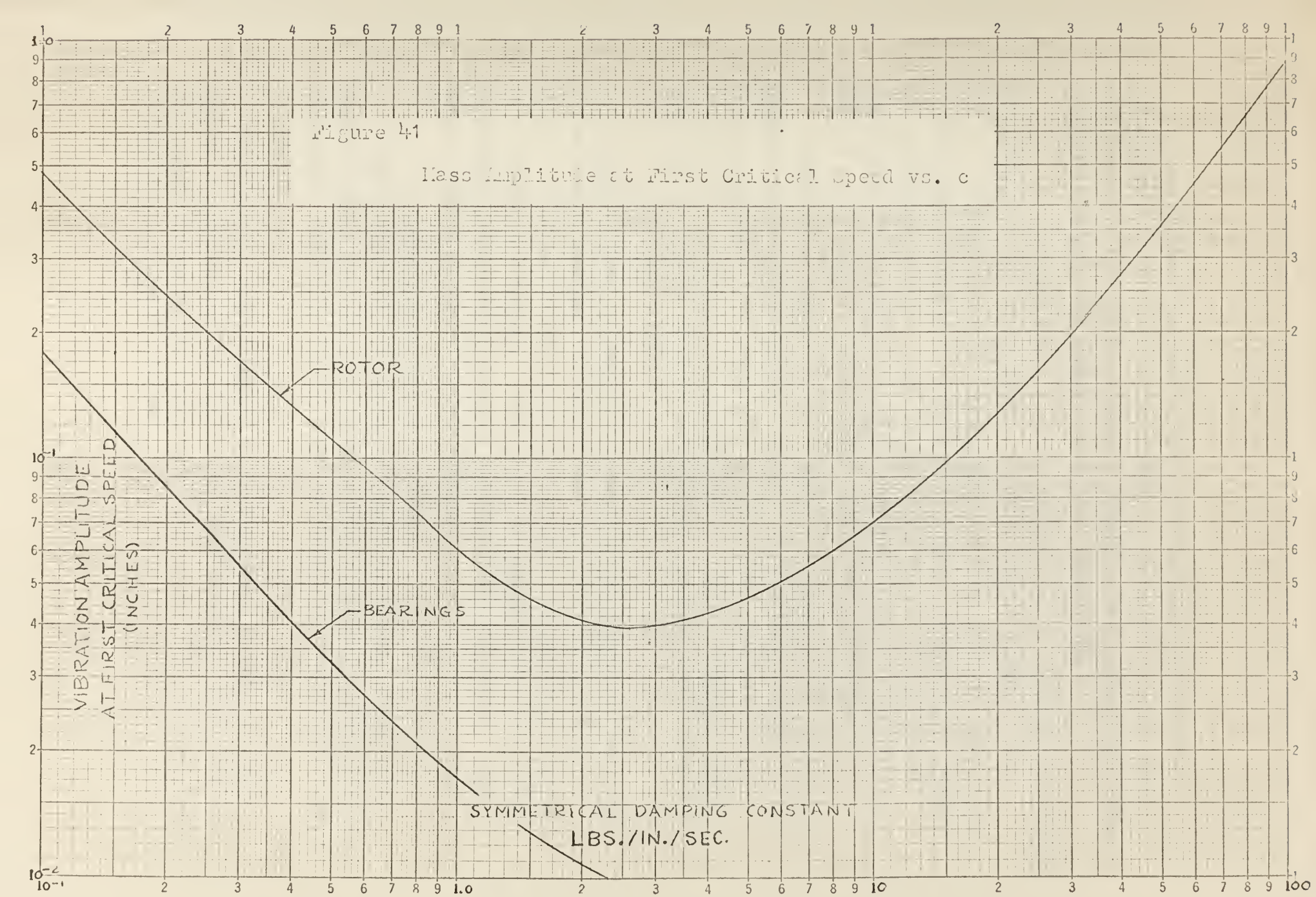
Figure 41
Mass Amplitude at First Critical Speed vs. c
ROTOR
BEARINGS
VIBRATION AMPLITUDE AT FIRST CRITICAL SPEED (INCHES)
SYMMETRICAL DAMPING CONSTANT
LBS./IN./SEC.

Figure 24 shows the modes of the three critical speeds for the undamped case. The calculated amplitudes of the masses at these three frequencies are not infinite because the exact values at which they occur were not assigned in the speeds selected for calculation.

As c is increased from 0.0 to 2.5 lbs./(in./sec.) the amplitude response of the masses at the first critical speed is seen to decrease. See Fig. 41. Responses at speeds higher than the first critical speed become less and less pronounced as damping is increased. Increasing the damping has a relatively greater effect on the amplitudes at critical speeds higher than the fundamental; once the damping exceeds 2.5 lbs./(in./sec.) there are virtually no critical speeds higher than the fundamental.

Comparison of Figures 35 and 37 shows a reversal in one trend of the response for increasing damping. Although the amplitude response of the bearings continues to decrease with higher damping, the rotor response is larger at 3.0 than at 2.5 lbs./(in./sec.). For the strongly damped case shown in Fig. 39 the rotor response has increased greatly over that for the lightly damped cases.

Figure 41 shows the amplitude response of the masses as a function of the damping constant. It can be seen that the value of 2.5 lbs./(in./sec.) constitutes that value of c for which the amplitude response of the system is a minimum. From this it is apparent that, under these conditions, maximum energy is being dissipated from the system. This case is defined as that of optimum damping.

4.2.3 Discussion of Theoretical Results

Figures 40 and 41 show the major effects of damping on the system. Figure 40 shows that the critical speed depends directly on the magnitude of damping. Similarly, Fig. 41 shows the dependence of amplitude response on damping.

The limiting case of damping on critical speed is that for which damping is infinite, or, in other words, fixed supports. The system is then reduced to one of the single mass of the rotor. The calculated value of this critical speed is 392 RPM.

In order to complete the description of the system at each value of damping, phase angle diagrams are included with each figure showing amplitude response. Somewhat contrary to the behavior of the spring-mass-dashpot system, the system considered shows a marked dependence of critical speed on damping, and the amplitude response is not always in inverse proportion to the damping.

4.3 Comments on the Theoretical Analysis

In general, the theoretical results appear to be valid and consistent with established theory. In confirmation of this, a simple, if limited, check on the method of calculation is presented.

For the case of fixed supports, Prohl, [2],

N_1 = first critical speed, RPM

k = shaft spring constant, lbs./in.

W = rotor weight, lbs.

$$N_1 = 187.7\ (k/W)^{\frac{1}{2}}\ \text{RPM}$$

$$= 187.7\ (66.5/15.21)^{\frac{1}{2}} = 392.3\ \text{RPM}$$

The calculated critical speed for this configuration was 392 RPM.

5. COMPARISON OF THEORETICAL AND EXPERIMENTAL RESULTS

Figure 31 shows the calculated and test amplitude responses for the case of damping of 1.77 lbs./(in./sec.).

The observed critical speed was 383 RPM. From Fig. 40, First Critical Speed vs. c, the critical speed corresponding to c = 1.77 lbs./(in./sec.) is 346, a discrepancy of 37 RPM. Also from Fig. 40, a critical speed of 383 RPM corresponds to a damping factor of 6.5 lbs./(in./sec.). From analysis of the observed critical speed there is the indication that the damping during the test was greater than that of 1.77 lbs./(in./sec.) thought to have been in effect.

Amplitude indications from the test were analyzed in conjunction with Fig. 41, Mass Amplitude at First Critical Speed vs. c. From the figure it can be seen that an amplitude of 0.116 corresponds with either of two damping constants, 0.047 or 18.0 lbs./(in./sec.). The lower value is felt to be totally improbable. The higher value, although excessive in itself, tends to confirm the indication noted in comparison of critical speeds that the damping was larger than 1.77 lbs./(in./sec.). Amplitude measurement error, although possibly greater at critical speeds due to transients from non-steady drive, could not account for the large discrepancy.

The apparent discrepancy in dashpot damping could stem from any of several sources. The dashpots may have been cocked during the run and produced a strong non-linear response. The dashpots were mounted vertically for their calibration. Their operation in the horizontal plane during the critical speed test may have produced the apparent change in their characteristics.

Figure 39 shows the calculated and experimental response for the fixed-bearing case. The calculated critical speed was 392 while the experimental value was 380. Since amplitudes are theoretically infinite for the fixed-bearing case, comparison is not applicable as in the case with lightly damped bearings. Based solely on the comparison of critical speeds the agreement between calculated and test results is fair.

6. CONCLUSIONS

The system of a rotor mounted on a shaft with damped and flexibly supported end bearings shows its amplitude response to be dependent on bearing support impedance. Rotor amplitudes decreased as damping increased to the optimum value of 2.5 lbs./(in./sec.) and increased for larger values of damping. There is a limit to which rotor amplitude at critical speeds can be influenced by damping at the bearings and one critical speed will persist in spite of damping applied.

The calibrated damping characteristics of the dashpots were either in error or dashpot damping was effected by the mechanical arrangement of the dashpots on the critical speed rig.

Accuracy of test measurements could be improved.

7. RECOMMENDATIONS

The critical speed test rig offers promise for use in further vibration analyses if improvements in its damping and control characteristics can be effected.

It is recommended that the physical system be improved by

a. Modification of the drive system to eliminate thrust along the shaft axis,
b. Design of a support for spring-spring holder assembly to permit testing without dashpots,
c. Provision of springs with stiffnesses between those of the springs tested, and
d. Use of better speed and amplitude indicators.

It is also recommended that a further investigation of the damping range and characteristics of the dashpots be conducted.

8. REFERENCES AND BIBLIOGRAPHY

Ref. 1: Prohl, M. A.: A general Method for Calculating Critical Speeds of Flexible Rotors. The Journal of Applied Mechanics, September, 1945.

Ref. 2: Prohl, M. A. and Linn, F. C.: The Effect of Flexibility of Support Upon the Critical Speeds of High-Speed Rotors. The Society of Naval Architects and Marine Engineers, Transactions, Vol. 59, 1951.

Ref. 3: DiTaranto, R. A.: Natural Frequencies of Non-Uniform Beams on Multiple Elastic Supports. The Journal of Applied Mechanics, March, 1958.

Ref. 4: Koenig, E. C., Guenther, T. G., and Lovejoy, D.C.: Analysis for Calculating Lateral Vibration Characteristics of Rotating Systems With Any Number of Flexible Supports. The Journal of Applied Mechanics, December, 1961.

Ref. 5: Manley, B. G.: Fundamentals of Vibration Study. 1942, Chapman and Hall, London.

Ref. 6: Machinery's Handbook. 1946, 13th ed., Industrial Press, New York.

Ref. 7: Smith, D. M.: The Motion of a Rotor Carried by a Flexible Shaft in Flexible Bearings. The Royal Society of London, Proceedings, 1933, Vol. 142 A.

Ref. 8: Alcoa Structural Handbook. 1955, Aluminum Company of America, Pittsburg, Pennsylvania.

Ref. 9: Perry, C. C. and Lissner, H. R.: The Strain Gage Primer. 1955, McGraw-Hill Book Company, Inc., New York, Toronto and London.

Ref. 10: Military Specification H-5606A of 21 February, 1957 superseding MIL-O-5606 of 31 January, 1950.

Ref. 11: Fortran System for the Control Data 1604 Computer. 1961, Computer Division, Control Data Corporation, Minneapolis, Minnesota.

Ref. 12: Burton, Ralph: Vibration and Impact. 1958, Addison-Wesley Publishing Company, Inc., Reading Massachusetts.

Bibliography of pertinent material used but not referred to specifically in the text.

Bishop, R. E. D.: Vibration of Rotating Shafts. Mechanical Engineering Science, Journal, 1959, Vol. No. 1.

Bishop, R. E. D. and Gladwell, G. M. L.: The Vibration and Balancing of an Unbalanced Flexible Rotor. Mechanical Engineering Science, Journal, 1959, Vol. 1, No. 1.

Den Hartog, J. P.: Mechanical Vibrations. 1956, 4th ed., McGraw-Hill Book Company, Inc., New York.

Dunkerley, S.: On the Whirling and Vibration of Shafts. Philosophical Transactions of the Royal Society of London, 1894, Vol. 185, series A.

Gladwell, G. M. L. and Bishop, R. E. D.: Vibration of Rotating Shafts Supported in Flexible Bearings. Mechanical Engineering Science, Journal, 1959, Vol. 1, No. 3.

Harris, Cyril M. and Crede, Charles E.: Shock and Vibration Handbook, Vol. 2. 1961, McGraw-Hill Book Company, Inc., New York.

Mabie, Hamilton H. and Ocvirk, Fred W.: Mechanisms and Dynamics of Machinery. 1957, John Wiley and Sons, Inc., New York.

Myklestad, N. O.: Vibration Analysis. 1944, 1st ed., McGraw-Hill Book Company, Inc., New York.

Norris, Charles H. et al: Structural Design for Dynamic Loads. 1959, McGraw-Hill Book Company, Inc., New York.

Southwell, R. V.: An Introduction to the Theory of Elasticity. 1941, 2nd ed., Oxford University Press, London.

Timoshenko, S. and Young, D. H.: Advanced Dynamics. 1948, McGraw-Hill Book Company, Inc., New York.